Nitrous Oxide State Estimation in Hybrid Rocket Oxidizer Tanks

by

Steven Borgdorff

A thesis
presented to the University of Waterloo
in fulfillment of the
thesis requirement for the degree of
Master of Applied Science
in
Mechanical and Mechatronics Engineering

Waterloo, Ontario, Canada, 2017

I hereby declare that I am the sole author of this thesis. This is a true copy of the thesis, including any required final revisions, as accepted by my examiners.

I understand that my thesis may be made electronically available to the public.

Abstract

There is an increasing interest in the use of hybrid rockets to accomplish tasks that require precise control of the craft. Fuel is being consumed as the craft is propelled, causing the mass of the rocket to change. In some hybrid rocket architectures, it is not possible to directly measure the mass of the oxidizer while the rocket is in flight. Further, controlling the flow rate of oxidizer is a method employed to control the overall thrust developed by a hybrid rocket. It is therefore important to understand how the changing state of the oxidizer may influence the mass flow rate of the oxidizer. For precise flight trajectory control, accurate estimates of the various states, including the mass of the rocket and remaining propellant are required.

Nitrous oxide is frequently selected as an oxidizer as it is relatively safe to store and handle, plus it is self pressurizing. Both of these advantages reduce complexity and cost and increase safety in a rocket program.

In theory, the mass of the rocket could be estimated with a very precise model. In practice, such models have not provided a satisfactory level of accuracy when estimating the remaining mass of oxidizer. The goal of this thesis is to accurately estimate the current mass of the oxidizer in the tank over time. The approach to solving this problem uses an Extended Kalman Filter to merge a model of the system states with available measurements of system states.

An existing model is selected, analyzed and discussed. It assumes the gas phase of nitrous oxide approximates an ideal gas, and that the gas and liquid phases are saturated in isothermal and isobaric equilibrium. Some alterations to this model are proposed as they are found to increase the accuracy. The changes include a first-order delay in the flow through the injector and the system components included in the modeled thermal mass are modified.

The model, and the available measurements are then implemented in an Extended Kalman Filter (EKF). The primary intent of the filter is to dynamically estimate the mass and properties of the oxidizer remaining in the rocket during flight. The EKF relies on updated measurements of the pressure in the oxidizer tank and the combustion chamber. The EKF discussed in this work is designed with the intent the flow rate of oxidizer can be controlled, and a dedicated flow rate control factor is included. However, the hardware for control systems for the mass flow rate are not a focus of this work.

The EKF performance is simulated and measured based on data collected from ground testing. An improvement over the use of simulation alone is demonstrated.

Acknowledgements

Above all, I must thank and give all praise to my Creator and Saviour for all the people and blessings in my life.

I am very grateful for for my parents, Leonard and Phyllis, for their love and support. My sister, Kate, and brother-in-law Roger have also helped in encouraging me to see this through to completion. My Grandparents and wider family and close friends have also been supportive of my pursuit.

On the academic side, I am very thankful for the time and flexibility of Professor Waslander who has generously worked around my schedule, provided prompt, honest, and encouraging feedback. He has supplied me with wisdom and knowledge throughout this endeavor. My friends from the University of Waterloo Rocketry team, Isaac Jourard, Ali Karimi, and Ben Criger have all contributed greatly to my interest in rockets. Together, we shared in the adventure of designing, building, testing, re-building, and launching a hybrid rocket.

I am thankful to the team I work with at Husky Injection Molding Systems in Bolton, Ontario for allowing me with a flexible work schedule to complete my studies and thesis.

Lastly, I must thank Rachel Houter. She has lovingly encouraged, supported, inspired and motivated me while working on this project, and in all areas of my life. Of all people and blessings in my life, I am most grateful to her and for her. I am excited to start our married life together soon!

Dedication

This is dedicated to God, my family, and certainly to Rachel. Thank you all.

Table of Contents

List of Tables viii

List of Figures ix

Nomenclature xiii

1 Introduction 1

2 Background 5

2.1 Saturated Nitrous Oxide Properties 7

2.2 Initializing the System States 8

2.3 Model Governing Equations and Implementation 9

2.4 Discussion of Original Model Results 11

3 Ideal Gas Modified Model 20

3.1 Ideal Gas Modified Model - Delay and Mixture Ratio 20

3.1.1 Injector Opening Delay τ 21

3.1.2 Nitrous Oxide Outflow Mixture Ratio ζ 22

3.1.3 Nitrous Oxide Evaporation Rate 23

3.1.4 Implementation of the Model 25

3.1.5 Optimization of Delay τ and Mixture Ratio ζ 25

3.2 Ideal Gas Modified Model - Delay, Mixture Ratio and Tank Thermal Mass 29

3.3 Discussion of Modified Model Results 35

4 Derivation of Extended Kalman Filter **46**

4.1 Initializing the System States 47

4.2 System Model 48

4.2.1 Nitrous Oxide Equilibrium Properties 48

4.2.2 Nitrous Oxide Outflow Rate and Evaporation Rate 49

4.2.3 State Updates 49

4.3 Jacobian of the System Model 50

4.3.1 Partial Derivatives of Mass Outflow Rate 50

4.3.2 Partial Derivatives of Oxidizer Evaporation Rate 51

4.3.3 Jacobian of the System Model 56

4.4 Extended Kalman Filter Structure 57

4.5 Identifying Uncertainty for State and Measurement Updates 58

4.6 Results of the Extended Kalman Filter 59

5 Conclusions and Recommendations **66**

5.1 Model Modifications 66

5.2 Extended Kalman Filter 67

5.3 Future Potential Refinements 67

5.4 Final Remarks 68

References **69**

List of Tables

3.1 Summary of optimized τ and ζ values 34

List of Figures

1.1 Basic diagram and components of a hybrid rocket engine with oxidizer flow rate control 2

2.1 Visual description of the assumptions made in the Original Ideal Gas Model 6
2.2 Oxidizer mass - Case 2: comparison of Original Ideal Gas Model simulation and testing results 12
2.3 Oxidizer mass - Case 3: comparison of Original Ideal Gas Model simulation and testing results 13
2.4 Pressure in the oxidizer tank - Case 2: comparison of Original Ideal Gas Model Pressure simulation and testing results 14
2.5 Pressure in the oxidizer tank - Case 3: comparison of Original Ideal Gas Model Pressure simulation and testing results 14
2.6 Oxidizer temperature - Case 2: comparison of Original Ideal Gas Model simulation and temperature assuming saturation pressure 15
2.7 Oxidizer temperature - Case 3: comparison of Original Ideal Gas Model simulation and temperature assuming saturation pressure 16
2.8 Moles of oxidizer phases - Case 2: Original Ideal Gas Model moles simulation 17
2.9 Moles of oxidizer phases - Case 3: Original Ideal Gas Model moles simulation 17
2.10 Oxidizer outflow density - Case 2: Original Ideal Gas Model Density from simulation compared to estimated density from outflow equation 18
2.11 Oxidizer outflow density - Case 3: Original Ideal Gas Model Density from simulation compared to estimated density from outflow equation 19

3.1 Visual description of the assumptions made in the first version of the Modified Ideal Gas Model 21

3.2 Oxidizer mass - Case 2: comparison of Modified Model with Delay and Mixture Ratio (MM-D,MR), Original Ideal Gas Model (OIGM), and testing results . . . 27

3.3 Pressure in oxidizer tank - Case 2: comparison of Modified Model with Delay and Mixture Ratio (MM-D,MR), Original Ideal Gas Model (OIGM), and testing results . . . 28

3.4 Oxidizer temperature - Case 2: comparison of Modified Model with Delay and Mixture Ratio (MM-D,MR), and Original Ideal Gas Model (OIGM) estimations assuming saturation pressure . . . 29

3.5 Pictorial description of the assumptions made in the second version of the Modified Ideal Gas Model where the thermal mass of the oxidizer tank is removed . . . 30

3.6 Oxidizer mass history - Case 2: comparison of Modified Model with Delay, Mixture Ratio and oxidizer tank Thermal Mass removed(MM-D,MR,TM), Original Ideal Gas Model (OIGM), and testing results; the model is optimized to reduce the error in the mass history . . . 31

3.7 Pressure in oxidizer tank - Case 2: comparison of Modified Model with Delay, Mixture Ratio and oxidizer tank Thermal Mass removed(MM-D,MR,TM), Original Ideal Gas Model (OIGM), and testing results; the model is optimized to reduce the error of the mass history . . . 32

3.8 Oxidizer mass - Case 2: comparison of Modified Model with Delay, Mixture Ratio and oxidizer tank Thermal Mass removed(MM-D,MR,TM), Original Ideal Gas Model (OIGM), and testing results; the simulation is optimized to minimize the error of the pressure history . . . 33

3.9 Pressure in oxidizer tank - Case 2: comparison of Modified Model with Delay, Mixture Ratio and oxidizer tank Thermal Mass removed(MM-D,MR,TM), Original Ideal Gas Model (OIGM), and testing results; the model is optimized to minimize the error of the pressure history . . . 34

3.10 Oxidizer mass - Case 2: comparison of Modified Model with Delay, Mixture Ratio and oxidizer tank Thermal Mass removed(MM-D,MR,TM), Original Ideal Gas Model (OIGM), and testing results . . . 36

3.11 Oxidizer mass - Case 3: comparison of Modified Model with Delay, Mixture Ratio and oxidizer tank Thermal Mass removed(MM-D,MR,TM), Original Ideal Gas Model (OIGM), and testing results . . . 37

3.12 Pressure in oxidizer tank - Case 2: comparison of Modified Model with Delay, Mixture Ratio and oxidizer tank Thermal Mass removed(MM-D,MR,TM), Original Ideal Gas Model (OIGM), and testing results; the model compromises between low error in both mass and pressure histories 38

3.13 Pressure in oxidizer tank - Case 3: comparison of Modified Model with Delay, Mixture Ratio and oxidizer tank Thermal Mass removed(MM-D,MR,TM), Original Ideal Gas Model (OIGM), and testing results; the model compromises between low error in both mass and pressure histories 39

3.14 Oxidizer temperature - Case 2: comparison of Modified Model with Delay, Mixture Ratio and oxidizer tank Thermal Mass removed(MM-D,MR,TM) and Original Ideal Gas Model (OIGM) estimations assuming saturation pressure; the model compromises between low error in both mass and pressure histories 40

3.15 Oxidizer temperature - Case 3: comparison of Modified Model with Delay, Mixture Ratio and oxidizer tank Thermal Mass removed(MM-D,MR,TM) and Original Ideal Gas Model (OIGM) estimations assuming saturation pressure; the model compromises between low error in both mass and pressure histories 41

3.16 Moles of oxidizer phases - Case 2: comparison of Modified Model with Delay, Mixture Ratio and oxidizer tank Thermal Mass removed(MM-D,MR,TM) and Original Ideal Gas Model (OIGM) estimations 42

3.17 Moles of oxidizer phases - Case 3: comparison of Modified Model with Delay, Mixture Ratio and oxidizer tank Thermal Mass removed(MM-D,MR,TM) and Original Ideal Gas Model (OIGM) estimations 43

3.18 Oxidizer outflow density - Case 2: comparison of Modified Model with Delay, Mixture Ratio and oxidizer tank Thermal Mass removed(MM-D,MR,TM) and Original Ideal Gas Model (OIGM) estimations 44

3.19 Oxidizer outflow density - Case 3: comparison of Modified Model with Delay, Mixture Ratio and oxidizer tank Thermal Mass removed(MM-D,MR,TM) and Original Ideal Gas Model (OIGM) estimations 45

4.1 Oxidizer mass - Case 2: comparison of Extended Kalman Filter (EKF) and testing results 60

4.2 Oxidizer mass - Case 3: comparison of Extended Kalman Filter (EKF) and testing results 60

4.3 Pressure in oxidizer tank - Case 2: comparison of Extended Kalman Filter (EKF) and testing results 61
4.4 Pressure in oxidizer tank - Case 3: comparison of Extended Kalman Filter (EKF) and testing results 62
4.5 Oxidizer temperature - Case 2: comparison of Extended Kalman Filter (EKF) and estimations of temperature assuming saturation pressure 63
4.6 Oxidizer temperature - Case 3: comparison of Extended Kalman Filter (EKF) and estimations of temperature assuming saturation pressure 63
4.7 Moles of oxidizer phases - Case 2: Extended Kalman Filter (EKF) estimations 64
4.8 Moles of oxidizer phases - Case 3: Extended Kalman Filter (EKF) estimations 65

Nomenclature

$\Delta\hat{H}_o$	Enthalpy of evaporation	[J/kmol]
$\frac{dP_o^{sat}}{dT}$	Saturated pressure rate of change with respect to Temperature Change of nitrous oxide	[bar/K]
$\dot{n}_{o,f}$	Rate of nitrous oxide leaving oxidizer tank	[kmol/s]
$\dot{n}_{o,g}$	Rate of nitrous oxide gas change in oxidizer tank	[kmol/s]
$\dot{n}_{o,l}$	Rate of nitrous oxide liquid change in oxidizer tank	[kmol/s]
$\dot{n}_{o,v}$	Rate of nitrous oxide evaporating in oxidizer tank	[kmol/s]
$\dot{T}_T$	Rate of temperature change of oxidizer tank system	[K/s]
$\hat{C}_{Vo,g}$	Specific energy of nitrous oxide gas	[J/(kg K)]
$\hat{C}_{Vo,l}$	Specific energy of nitrous oxide liquid	[J/(kg K)]
$\hat{V}_{o,l}$	Specific volume of nitrous oxide liquid	[m^3/kg]
ρ_f	Density of nitrous oxide leaving oxidizer tank	[kg/m^3]
$\rho_{o,g}$	Density of nitrous oxide gas	[kg/m^3]
$\rho_{o,l}$	Density of nitrous oxide liquid	[kg/m^3]
τ	Time constant of initial injector behavior	[s]
$\tilde{y}_k$	EKF Measurement residual vector at discrete time step	[–]
ζ	Ratio of nitrous oxide gas moles at injector to total moles at injector	[kmol/kmol]

A_{inj}	Injector cross-section area	[m^2]
C_D	Injector flow coefficient	[–]
F_k	EKF system model Jacobian Matrix at a discrete time step	[–]
H_k	EKF Measurement Jacobian Matrix	[–]
k	EKF discrete time step	[s]
K_k	EKF near-optimal Kalman gain at discrete time step	[–]
m_T	mass of the oxidizer tank	[kg]
M_o	Molar mass of nitrous oxide	[44.013 kg/kmol]
m_o	Mass of nitrous oxide in oxidizer tank	[kg]
n_{He}	Moles of helium	[kmol]
$n_{o,g}$	Moles of nitrous oxide gas	[kmol]
$n_{o,l}$	Moles of nitrous oxide liquid	[kmol]
P_o^{sat}	Saturated pressure of nitrous oxide	[bar]
P_C	Pressure in Combustion Chamber	[bar]
P_T	Pressure in oxidizer tank	[bar]
Q_k	EKF estimate of process noise	[–]
R	Universal gas constant	[8314.3 J/(kmol*K)]
R_k	EKF Gaussian measurement noise at discrete time step	[–]
S_k	EKF innovation covariance at discrete time step	[–]
T	Temperature	[K]
T_T	Temperature of oxidizer tank system	[K]
u_k	EKF control vector at a discrete time step	[–]
x_k	EKF state vector at a discrete time step	[–]
y_k	EKF measurement vector at a discrete time step	[–]

Chapter 1

Introduction

Rockets have opened up many new opportunities and possibilities in the fields of science, communications, navigations, and transportation [1]. There are three main types of rocket propulsion used in launch vehicles and they are solid fuel, liquid bipropellant, and hybrid rockets [2] [1]. This thesis focuses on the hybrid rocket. This type of rocket can be used to launch small satellites, to explore the upper atmosphere, as test beds for supersonic aerodynamic tests [3], and even manned flight.

Hybrid rockets are typically designed to have a solid fuel, and a liquid or gaseous oxidizer. The oxidizer is typically self-pressurizing, such as nitrous oxide, and therefore does not require a pump to force it into the combustion chamber. The solid fuel is commonly stored in the combustion chamber and requires an oxidizer to sustain combustion. The oxidizer and the fuel are generally stable separately. The use of different phases means accidental contact of the oxidizer and fuel carries a low combustion or explosion risk compared to liquid bi-propellents. Solid rocket motors carry higher storage risks as the fuel and oxidizer are mixed together in fuel grain; thus great care is required to keep accidental sparks or heat sources from causing undesired ignition of the motor. The hybrid engine generally requires an ignition source to initiate combustion when mixed. This leads to a relatively high degree of inherent safety. These qualities also allow hybrid rockets to be stored in a relatively safe manner [1]. They can be designed to operate with a wide variety of fuels and oxidizers, many of which produce no harmful biproducts during combustion, meaning low risk of damage to the environment [4]. Hybrid rocket engines can also be designed for stop and restart operation. The thrust can be controlled by throttling the flow of oxidizer into the combustion chamber as described in [5] and [6]. This architecture is attractive compared to the liquid bi-propellants because of reduced design and manufacturing complexity while maintaining much of the functionality. Due to the oxidizer

and fuel being stored in different phases (generally solid fuel and gas or liquid oxidizer), hybrid rockets reduce the potential safety hazards present in solid rocket motors and liquid bi-propellant engines. The basic arrangement of components is described in 1.1.

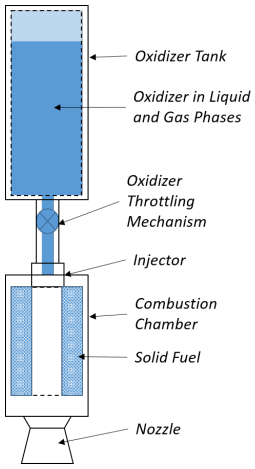

Figure 1.1: Basic diagram and components of a hybrid rocket engine with oxidizer flow rate control

Nitrous oxide is commonly used as an oxidizer in hybrid rockets. It is relatively economical and facilitates a relatively simple engine design. It can be stored at room temperature in a high pressure liquid-gas mixture. The vapor pressure is sufficient to drive flow of the oxidizer into the combustion chamber without the use of a pump. Accurately modelling the properties of nitrous oxide is a significant challenge as the high pressure and interactions between the phases reduce the accuracy of ideal gas law assumptions. Various models for oxidizer tanks have been proposed and compared to test data [7].

These technical benefits of hybrid rockets translate into financial benefits and there is a demand for low cost launch vehicles. The inherent safety characteristics reduce the financial costs of a launch vehicle immensly. The hybrid engine also uses fuels and oxidizers that are available at low cost and can be safely stored for long periods of time. This reduces the security and infrastructure required at the launch facility. The infrastructure for the oxidizer and fuel delivery systems avoid the use of turbopumps as are found in liquid bipropellants. Further research is being placed into the use of the sensors and guidance systems available off-the-shelf [8]. Given the previously mentioned benefits of hybrid rockets, coupled with the low cost, these are being investigated as an attractive option for launching many small satellites into LEO, boosters on larger rockets, student satellites and upper-atmosphere experiments [9].

The primary trade-off of hybrid rockets is reduced performance due to a low burn rate. This has limited the use of hybrid engines with a single port on the fuel grain to small scale applications, and has caused larger scale hybrid engines to contain multiple ports [10]. The multiple ports increase the surface area available for combustion, but it also increases the challenges of consistent manfacturing of the fuel grain. Advancements are being made on these challenges through research into the use of various fuel types that have significantly higher burn rates [11]. Large low-frequency pressure fluctuations can often be observed in the combustion chamber pressure history which is also a deterrent to the use of a hybrid engine [10] [12]. The fluctuations could potentially cause damage to sensitive and costly equipment transported in the rocket. Modelling and testing efforts that contribute to the understanding and reduction of these flutuations is ongoing and critical to the future use of hybrid engines [13]. Further, the dynamics of nitrous oxide, a common oxidizer selection for hybrid rockets, in a draining oxidizer chamber are especially difficult to model. This makes design of the oxidizer tank challenging to optimize without several costly testing iterations [14] [15] [7] [16]. The cost of conducting experiments that study the behavior of nitrous oxide have been reduced by using carbon dioxide in a similar blow-down situation [17]. Carbon dioxide shares similar critical properties to nitrous oxide that influence the blow down behavior [16] [15]. The challenges that face the acceptance and use of hybrid rockets are being investigated and mitigated through many ongoing projects in private industry, academia and government.

A plurality of models have been developed to attempt to describe the dynamics of nitrous oxide draining from an oxidizer tank. These have been compared for their ability to simlate experimental results in [16]. Recent advancements in the field have revealed that boiling of the fluid plays a critical role in the mass and heat transfer within the system [17]. This source also lays the groundwork for developing a model that considers many intricate features of boiling, but concedes that the model possibly carries the highest computational load. Greater model complexity is justified for detailed design and optimization of a hybrid rocket engine; however, the focus of this thesis is on in-flight estimations of mass. Therefore, the equilibrium and ideal gas model is primarily studied.

An in-flight knowledge of the mass of the rocket is required for thrust vectoring control. It is also required for dynamically determining the thrust required to meet other flight parameters as velocity and acceleration. For hybrid engines, the thrust can be varied by throttling the flow of oxidizer. The expected performance of the rocket can also be limited by the quantity of remaining oxidizer. For these reasons, control of the flight of the hybrid rocket depends on knowing the remaining mass in the oxidizer tank at all time points.

Kalman filters have been developed to combine a model of a system and related sensor inputs to determine optimal estimates of the system's states. Kalman Filters can operate

on linear systems. For non-linear systems, the system model can be linearized around an operating point and used to estimate system states near the operating point. If the system is to be operated through a range where it cannot be linearized on a single operating point, then an Extended Kalman Filter (EKF) may be implemented. Due to the large changes in the states of nitrous oxide, a model cannot be linearized around a single operating point, and therefore the use of an EKF is justly applied to this situation. The EKF takes a non-linear system model, and linearized estimates of the rate of change for the states, sensor inputs of related measurements, and develops a near-optimal estimate of the system states. Due to the use of first-order linearization, the EKF results cannot be said to be perfectly optimal; however, the estimates are still sufficient for good control in several practical implementations.

Chapter 2

Background

Several models to describe the dynamnics of nitrous oxide in an oxidizer tank have been developed. These are compared in [7] and [17]. In this thesis, an equilibrium and ideal gas model is primarily studied. Minor modifications are suggested that partially account for the boiling and possible cavitation effects. The original Ideal Gas Model presented by [14] is discussed in this section. This model is also used as part of a larger hybrid engine simulation in[18]. The model is based on the following assumptions:

- the gas phase of nitrous oxide is governed by ideal gas laws
- the gas molecules have negligible interactions with each other
- the liquid-vapor interactions are governed by Raoult's Law
- the nitrous oxide is always in thermal equilibrium, therefore the saturation properties are used to model the fluid
- there is a single interface between the gas and liquid phases evaporation occurs only at this interface
- if liquid nitrous oxide is present in the system, then only liquid is flowing through the injector

The assumptions are described visually in 2.1.

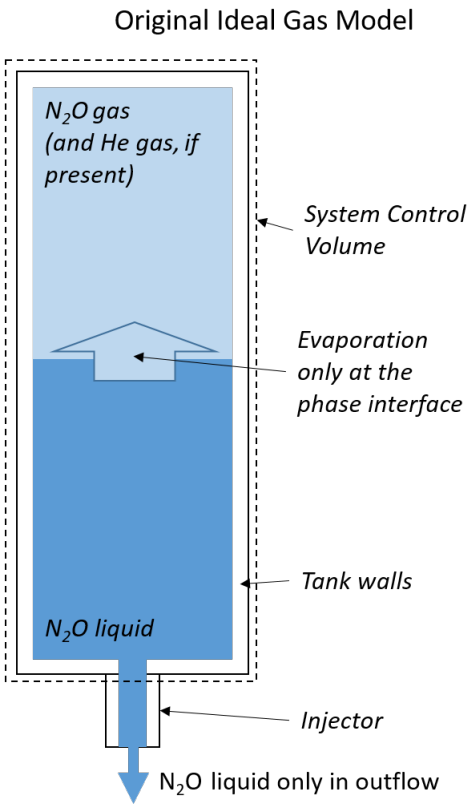

Figure 2.1: Visual description of the assumptions made in the Original Ideal Gas Model

2.1 Saturated Nitrous Oxide Properties

The saturation properties are used in the original ideal gas model. Saturated nitrous oxide properties are described as a function of temperature and are available in [19]:

$$
\begin{aligned}
P_o^{sat} &= f_1(T) && (2.1)\\
\hat{V}_{o,l} &= f_2(T) && (2.2)\\
\hat{C}_{Vo,l} &= f_3(T) && (2.3)\\
\hat{C}_{Vo,g} &= f_4(T) && (2.4)\\
\Delta\hat{H}_o &= f_5(T) && (2.5)\\
\frac{dP_o^{sat}}{dT} &= f_6(T) && (2.6)\\
& && (2.7)
\end{aligned}
$$

where:

- P_o^{sat} is the saturated pressure of nitrous oxide
- $\hat{V}_{o,l}$ is the specific volume of nitrous oxide liquid
- $\hat{C}_{Vo,l}$ is the specific energy of nitrous oxide liquid
- $\hat{C}_{Vo,g}$ is the specific energy of nitrous oxide gas
- $\Delta\hat{H}_o$ is the enthalpy of evaporation
- $\frac{dP_o^{sat}}{dT}$ is the rate of change of the nitrous oxide saturated pressure with respect to temperature
- T is temperature

The total tank pressure is described as a function of the number of nitrous oxide gas moles, helium gas moles and nitrous oxide saturation pressure. It is based on Raoults law for partial pressures of ideal gases. ([14] equations A.8 and A.9)

$$P_o^{sat} = \frac{n_{o,g}}{n_{o,g} + n_{He,g}} P_T \tag{2.8}$$

where:

- P_T is the pressure in the oxidizer tank
- $n_{o,l}$ is the number of moles of nitrous oxide liquid
- $n_{o,g}$ is the number of moles of nitrous oxide gas
- n_{He} is the number of moles of helium

2.2 Initializing the System States

The initial system states are based on the assumption that the system is in equilibrium. The initial mass of oxidizer in the oxidizer tank is determined by a measurement. In an actual rocket flight situation, the initial mass would be determined and initialized on the launch pad immediately before the firing of the engine. The initial oxidizer temperature might be based on a direct measurement of the oxidizer tank temperature in some architectures. In the data and models presented, the initial temperature is based on the assumption that the oxidizer is in equilibrium with the surrounding environment. The initial rate of temperature change is assumed to be zero. The number of oxidizer moles in the liquid and gas phases are determined by equilibrium relations. The initial oxidizer tank pressure in the model is based on the assumed number of gaseous oxidizer moles, a known amount of Helium (if any is added to the oxidizer) and the initial oxidizer temperature as shown in 2.2. The initial tank pressure is then obtained by rearranging equation 2.8.

The states with initial conditions set by measurement are stated below:

- m_{o_0} which is the initial mass of nitrous oxide in the oxidizer tank
- T_{T_0} which is the initial temperature in the oxidizer tank
- $\dot{T}_{T_0}$ which is the initial rate of temperature change in the oxidizer tank, assumed to be 0

The equations for determining the remaining state initial conditions are summarized

below:

$$P_{T_0} = \frac{n_{o,g_0} + n_{He}}{n_{o,g}} P_o^{sat} \tag{2.9}$$

$$n_{o,l_0} = \frac{\frac{m_{o_0}}{M_o} R T_{T_0} - P_o^{sat} V_T}{-P_o^{sat} \hat{V}_{o,l} + R T_{T_0}} \tag{2.10}$$

$$n_{o,g_0} = \frac{P_o^{sat}(V_T - \hat{V}_{o,l} \frac{m_{o_0}}{M_o})}{-P_o^{sat} \hat{V}_{o,l} + R T_{T_0}} \tag{2.11}$$

where:

- R is the universal gas constant
- M_o is the molar mass of nitrous oxide

2.3 Model Governing Equations and Implementation

The following equations describe the rates of change for the liquid oxidizer and oxidizer gas and are derived from the conservation of mass laws (from [14] A.1 and A.4):

$$\dot{n}_{o,l} = -\dot{n}_{o,f} - \dot{n}_{o,v} \tag{2.12}$$

$$\dot{n}_{o,g} = \dot{n}_{o,v} \tag{2.13}$$

where:

- $\dot{n}_{o,l}$ is the molar rate of change of the nitrous oxide liquid
- $\dot{n}_{o,g}$ is the molar rate of change of the nitrous oxide gas
- $\dot{n}_{o,f}$ is the total molar rate of nitrous oxide outflow from the tank
- $\dot{n}_{o,v}$ is the molar rate of nitrous oxide evaporation in the tank

The original model assumed that the fluid leaving through the injector was composed entirely of N2O liquid. The outflow density is not explicitly stated by [14], but it can be modeled as:

$$\rho_f = \rho_{o,l} = \frac{1}{\hat{V}_{o,l}} \tag{2.14}$$

where:

- ρ_f is the mass density of nitrous oxide outflow from the tank
- $\rho_{o,l}$ is the mass density of nitrous oxide liquid in the tank
- $\rho_{o,g}$ is the mass density of nitrous oxide gas in the tank (discussed later in the document)

The resulting outflow equation is presented in equation 2.15. It is a modified from the version presented in ([14] A.3) as the original focus is on the molar outflow form rather than mass outflow.

$$\dot{n}_{o,f} = C_D A_{inj} \sqrt{\frac{2(P_T - P_C)}{M_o \hat{V}_{o,l}}} \tag{2.15}$$

where:

- C_D is the injector flow coefficient
- A_{inj} is the injector cross-section area
- P_C is the pressure in the combustion chamber

This equation assumes that the flow through the injector depends on both the pressure of oxidizer and the combustion; that is, that flow through the injector does not exceed the speed of sound of the material travelling through the injector, and that the flow is incompressible [20]. Making this assumption for the flow of nitrous oxide is challenged in [15]. Further, there are ongoing investigations with injectors that deliberately cause the nitrous oxide to exceed the speed of sound [12]. This disconnects the hydrodynamic communication between the oxidizer tank and the combustion chamber, and may lead to greater combustion stability.

Nitrous oxide in an oxidizer tank evaporates as the liquid oxidizer leaves the tank. The reduced liquid volume increases the volume available for gas-phase oxidizer. Evaporation is modeled by assuming that the system maintains a thermal equilibrium throughout the draining process and the gas phase follows ideal gas behavior. The following equation is derived from the ideal gas law and the assumption that the nitrous oxide gas is at the saturation pressure:

$$P_o^{sat} V_{o,g} = n_{o,g} R T \tag{2.16}$$

The gas volume follows the following constraint as suggested in figure 2.1:

$$V_{o,g} = V_T - V_{o,l} \tag{2.17}$$

The the gas volume is substituted into equation 2.16 and the derivative with respect to time is then taken yielding the following equation ([14] A.16c):

$$- P_o^{sat}\hat{V}_{o,l}\dot{n}_{o,l} + (V_T - n_{o,l}\hat{V}_{o,l})\frac{dP_o^{sat}}{dT}\dot{T}_T = R(T_T\dot{n}_{o,v} + n_{o,g}\dot{T}_T) \tag{2.18}$$

Substitute 2.13 and 2.13:

$$- P_o^{sat}\hat{V}_{o,l}(-\dot{n}_{o,l} - \dot{n}_{o,v}) + (V_T - n_{o,l}\hat{V}_{o,l})\frac{dP_o^{sat}}{dT}\dot{T}_T = R(T_T\dot{n}_{o,v} + n_{o,g}\dot{T}_T) \tag{2.19}$$

Rearrange:

$$\dot{n}_{o,v} = \frac{(V_T - n_{o,l}\hat{V}_{o,l})\frac{dP_o^{sat}}{dT} - Rn_{o,g}}{RT_T - P_o^{sat}\hat{V}_{o,l}}\dot{T}_T + \frac{\hat{V}_{o,l}P_o^{sat}}{RT_T - P_o^{sat}\hat{V}_{o,l}}\dot{n}_{o,f} \tag{2.20}$$

The rate of temperature change is also required in order to model the dynamics of the system. For the original model, this is given with the following equation ([14] A.16a):

$$\dot{T}_T = \frac{(RT_T - \Delta\hat{H}_o)\dot{n}_{o,g} + (P_T\hat{V}_{o,l})\dot{n}_{o,l}}{m_T\bar{c}_{P_T} + n_{o,l}\hat{C}_{Vo,l} + n_{o,g}\hat{C}_{Vo,g} + n_{He}\hat{C}_{V,He}} \tag{2.21}$$

The model is then formulated into three derivative equations which are functions of three unknowns, and are solved simultaneously using an ODE solver in Mat Lab.

$$\begin{bmatrix} \dot{T}_T \\ \dot{n}_{o,l} \\ \dot{n}_{o,g} \end{bmatrix} = \begin{bmatrix} f_a(T_T, n_{o,l}, n_{o,g}) \\ f_b(T_T, n_{o,l}, n_{o,g}) \\ f_c(T_T, n_{o,l}, n_{o,g}) \end{bmatrix} \tag{2.22}$$

The pressure in the combustion chamber is modeled with a sixth-order polynomial fit to the measured pressure data. The polynomial equation facilitates the use of the ODE solver. This polynomial fit is developed by the author of [14] and is only used in this work to evaluate the original model. The further work presented in this thesis does not make use of an ODE solver; consequently, the polynomial fit also not used.

2.4 Discussion of Original Model Results

This section discusses the performance of the model compared to two sets of data. These are referred to as 'Case 2' and 'Case 3' and are both presented by [14] and the original

data is supplied in [21] and [22]. The results are presented here to demonstrate how the assumptions compare to the model results.

The original ideal gas model predicts the mass flow rate of the nitrous oxide to be higher than is recorded in the data from both tests. At the beginning of the test data, there is a short period of time where the mass shows little change. The presence of this delay is noted by [14]; however, the root cause is undetermined.

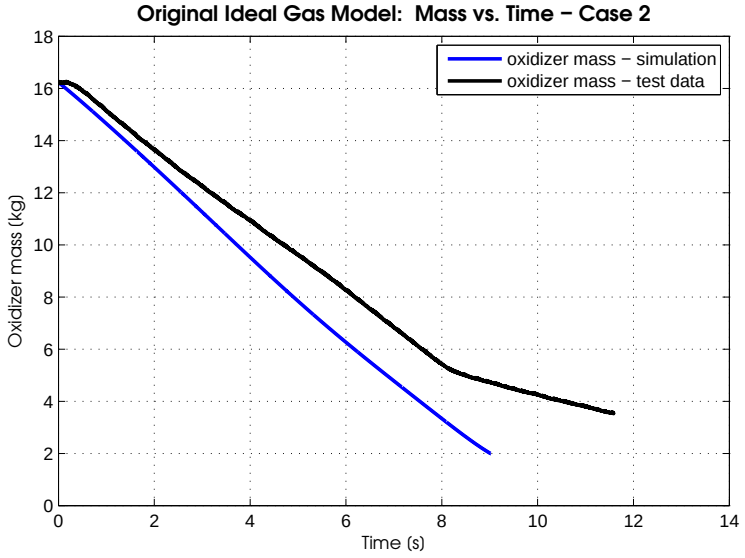

Figure 2.2: Oxidizer mass - Case 2: comparison of Original Ideal Gas Model simulation and testing results

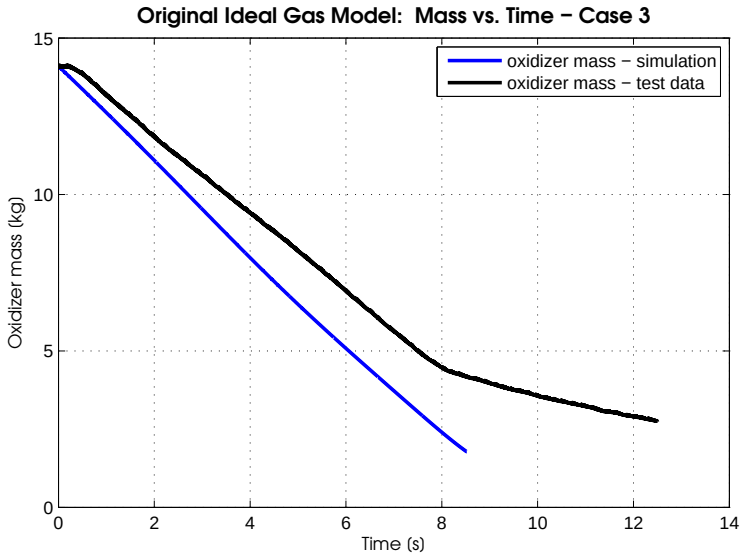

Figure 2.3: Oxidizer mass - Case 3: comparison of Original Ideal Gas Model simulation and testing results

The pressure data suggests that there are different trends in reality than is modeled. The pressure initially drops more rapidly in the data than in the model, then the rate of change slows as the amount of liquid nitrous oxide decreases.

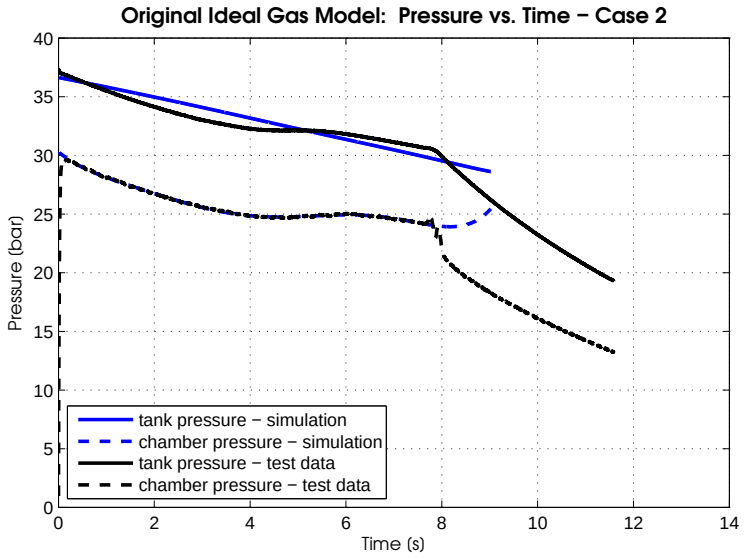

Figure 2.4: Pressure in the oxidizer tank - Case 2: comparison of Original Ideal Gas Model Pressure simulation and testing results

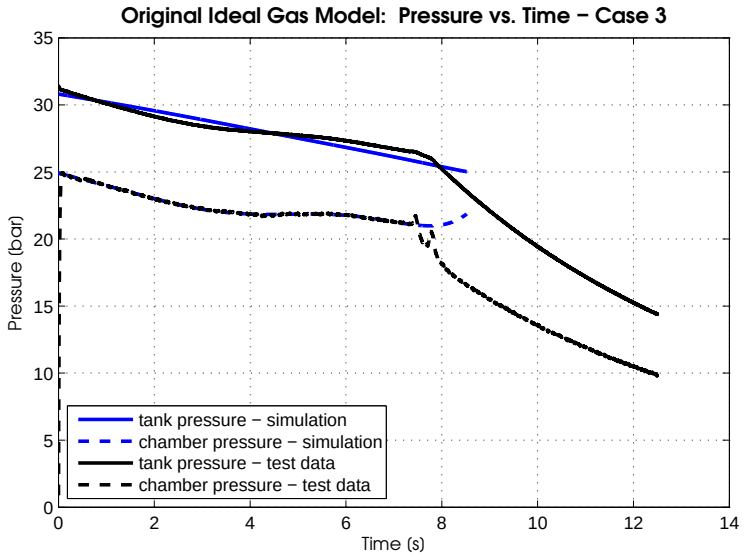

Figure 2.5: Pressure in the oxidizer tank - Case 3: comparison of Original Ideal Gas Model Pressure simulation and testing results

The temperature of the nitrous oxide is not measured. The temperature is estimated by assuming that the nitrous oxide is at saturation pressure and determining the corresponding temperature.

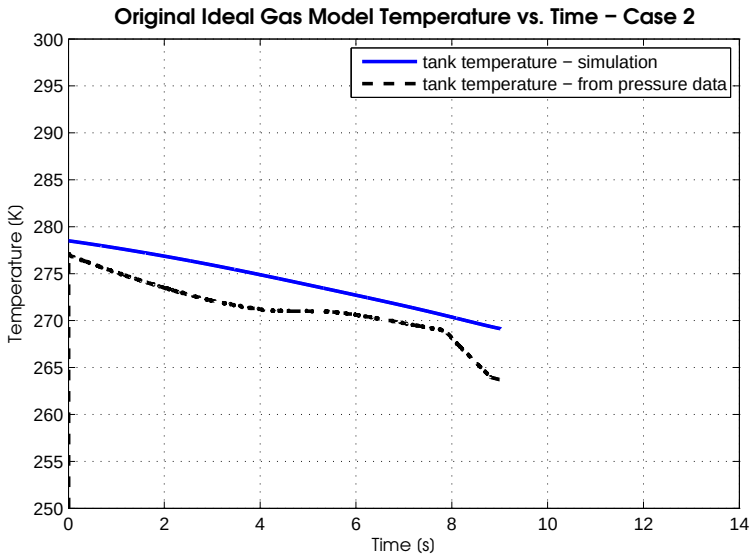

Figure 2.6: Oxidizer temperature - Case 2: comparison of Original Ideal Gas Model simulation and temperature assuming saturation pressure

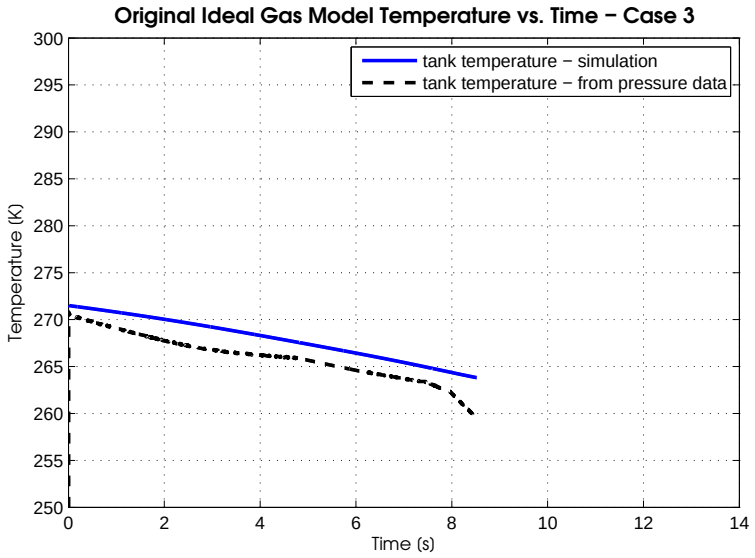

Figure 2.7: Oxidizer temperature - Case 3: comparison of Original Ideal Gas Model simulation and temperature assuming saturation pressure

The liquid and gas moles estimated to be in the system are shown in figures 2.8 and 2.9. The simulation time is ended when no liquid nitrous oxide is estimated to be present in the system. These figures demonstrate how the model simulates the increase in gas moles due to evaporation. The number of moles in both phases is not measured.

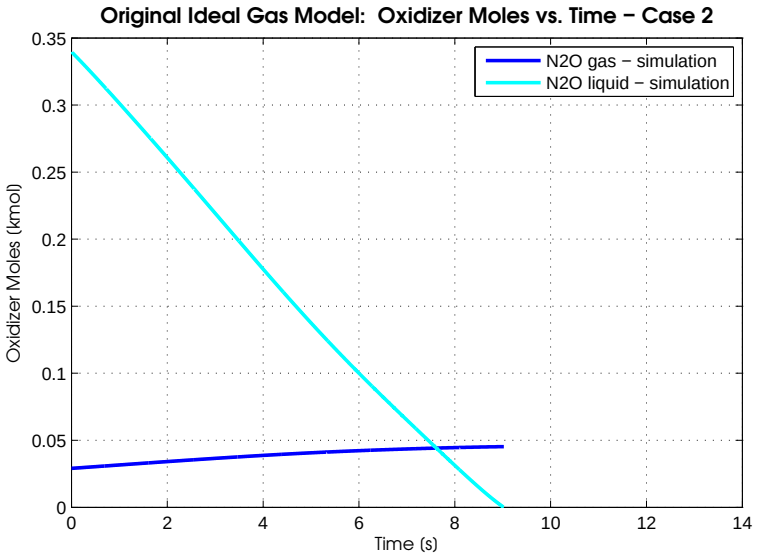

Figure 2.8: Moles of oxidizer phases - Case 2: Original Ideal Gas Model moles simulation

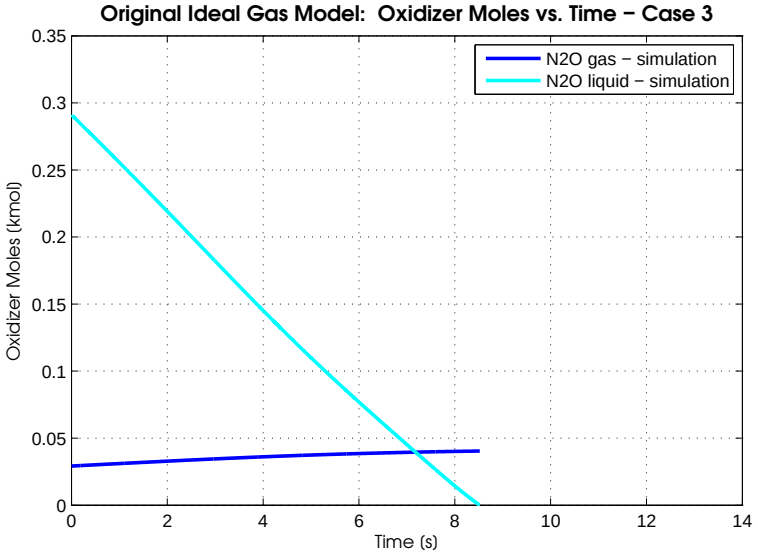

Figure 2.9: Moles of oxidizer phases - Case 3: Original Ideal Gas Model moles simulation

The actual density of the nitrous oxide outflow is estimated by rearranging equation

2.15 and substituting the known injector cross-sectional area and measured change of oxidizer mass in the oxidizer tank. The modeled outflow density is based on the temperature dependent liquid oxidizer properties. It is shown that the actual outflow density is significantly lower than the modeled outflow density.

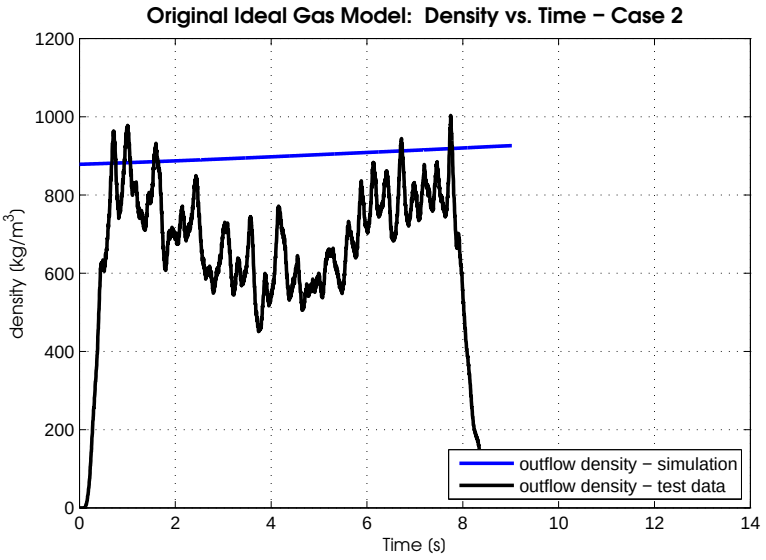

Figure 2.10: Oxidizer outflow density - Case 2: Original Ideal Gas Model Density from simulation compared to estimated density from outflow equation

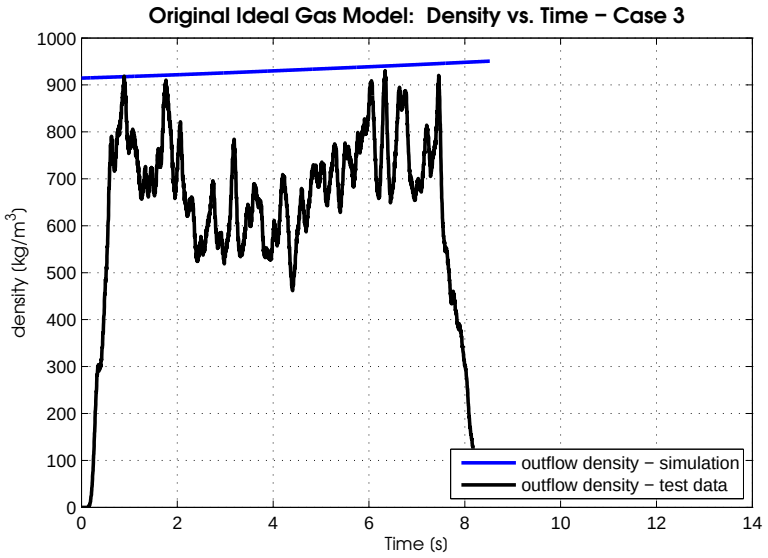

Figure 2.11: Oxidizer outflow density - Case 3: Original Ideal Gas Model Density from simulation compared to estimated density from outflow equation

The difference between the modeled density and the density suggested by the data may be explained by the presence of vapor in the outflow[23]. A multi-phase outflow of nitrous oxide through an injector is discussed in [15]. Multi-phase nitrous oxide flow is found to better estimate the actual mass outflow rate of the oxidizer.

Chapter 3

Ideal Gas Modified Model

The original Ideal Gas Model is intended to be used during the design phase of the rocket. It could be used to estimate performance of an engine using this tank. It is not intended to be used for estimating oxidizer properties during flight or for use in a control system. Consequently, the model does not presume that the oxidizer flow can be throttled. The Ideal Gas Model is modified in some minor ways to enable it to be used in a control system and these are described throughout the chapter. There are also two primary distinctions from the original Ideal Gas Model that are intended to reduce the error between the test data measurements and the model results. First, it is assumed that injector requires a small period of time to fully open. This is modeled with a delay. Second, it is assumed that a mixture of liquid oxidizer and oxidizer gas are exiting through the injector. This is modeled with a mixture ratio.

3.1 Ideal Gas Modified Model - Delay and Mixture Ratio

The modified model assumes that evaporation occurs throughout the liquid phase, turbulently forming many small gaseous regions, or bubbles. This is shown in figure 3.1 where boiling is happening throughout the liquid phase, and some of the gas phase bubbles are expelled in the oxidizer outflow.

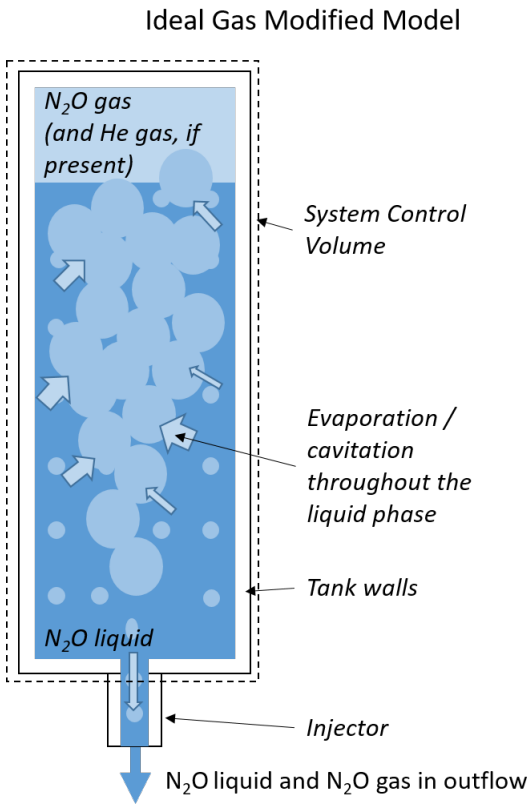

Figure 3.1: Visual description of the assumptions made in the first version of the Modified Ideal Gas Model

The potential presence of helium in the oxidizer tank is originally suggested by [14], and the resulting equations are carried over into this work. This work does not present any validation of a tank containing helium along with nitrous oxide. This is left as future potential work.

3.1.1 Injector Opening Delay τ

The delay in the opening of the injector is meant to account for the initial slow rate of nitrous oxide mass loss. This slow rate of mass loss can be observed at the very beginning of the recorded nitrous oxide mass data; however, the Original Ideal Gas model does not

account for this behavior. A simple first order relation is used to model this delay.

$$\dot{n}_{o,f} = C_D A_{inj} \sqrt{\frac{2(P_T - P_C)}{M_o \hat{V}_{o,l}}} \left(1 - \exp(\frac{-t}{\tau})\right) \tag{3.1}$$

Where τ is the time constant of the initial injector behavior.

3.1.2 Nitrous Oxide Outflow Mixture Ratio ζ

The modified model assumes that a mixture of gas and liquid oxidizer are leaving the tank simultaneously. This may be caused by cavitation or boiling in the injector system. The ratio of gas moles to total moles of oxidizer leaving the tank is described as ζ. The proposed ideal gas modified model assumes that ζ is constant while liquid oxidizer is still present in the tank. This assumption is made for the purpose of developing a model with certain level of simplicity and accuracy. This assumption does not address bubble formation variability or frequency. As a result of this assumption, the rates of change of the oxidizer liquid and gas phases are represented as the following:

$$\dot{n}_{o,l} = -(1-\zeta)\dot{n}_{o,f} - \dot{n}_{o,v} \tag{3.2}$$

$$\dot{n}_{o,g} = -\zeta\dot{n}_{o,f} + \dot{n}_{o,v} \tag{3.3}$$

The modeled nitrous oxide outflow density is described as the following:

$$\rho_f = \zeta\rho_{o,g} + (1-\zeta)\rho_{o,l} \tag{3.4}$$

The density of oxidizer gas is modeled with the ideal gas law. It is assumed that the helium gas (if present at all in the system) remains in the area of the initial ullage and further that no helium exits the tank while liquid oxidizer remains in the tank. The oxidizer gas exiting the tank is assumed to be from bubbles that form within the primarily liquid phase of the oxidizer near the injector port. These bubbles are assumed to be purely composed of the nitrous oxide and at the same pressure as the surrounding liquid phase. The liquid phase, and therefore these gas bubbles, are assumed to be equal to the total tank pressure. Therefore, the nitrous oxide in the gas phase at the injector port is assumed to be at the total tank pressure, not necessarily the partial pressure of the nitrous oxide at the temperature.

$$\rho_f = \zeta\frac{P_T}{RT_T} + (1-\zeta)\frac{1}{\hat{V}_{o,l}} \tag{3.5}$$

The pressure differential that drives flow is described below.

$$\Delta P = (P_T - P_C) \tag{3.6}$$

The outflow equation 3.1 becomes the following modified outflow density equation:

$$\dot{n}_{o,f} = C_D A_{inj} \sqrt{\left(\frac{2}{M_o}\right)(\rho_f)\,\Delta P}\left(1 - \exp(\frac{-t}{\tau})\right) \tag{3.7}$$

3.1.3 Nitrous Oxide Evaporation Rate

The equations describing the rate of oxidizer evaporation is determined for the modified model. The reader is reminded of equation 2.8:

$$P_o^{sat} = \frac{n_{o,g}}{n_{o,g} + n_{He,g}} P_T \tag{3.8}$$

To facilitate the derivation of the equations describing the evaporation rate, the following terms are defined:

$$\begin{aligned}
b_1 &= (V_T - n_{o,l}\hat{V}_{o,l})\frac{dP_o^{sat}}{dT} - Rn_{o,g} && (3.9)\\
b_{2,P_o^{sat}} &= RT_T - P_o^{sat}\hat{V}_{o,l} && (3.10)\\
b_{2,P_T} &= RT_T - \left(\frac{n_{o,g}}{n_{o,g} + n_{He}}\right) P_T\hat{V}_{o,l} && (3.11)\\
b_3 &= P_T\hat{V}_{o,l} - RT_T + \Delta\hat{H}_o && (3.12)\\
b_4 &= m_{Al,T}\bar{c}_{P_T} + n_{o,l}\hat{C}_{Vo,l} + n_{o,g}\hat{C}_{Vo,g} + n_{He}\hat{C}_{V,He} && (3.13)\\
b_5 &= \left(-\frac{n_{o,g}}{n_{o,g} + n_{He}}\right) P_T\hat{V}_{o,l} + \zeta b_{2,P_T} && (3.14)
\end{aligned}$$

Note that b_{2,P_T} is derived from $b_{2,P_o^{sat}}$ and substituting equation 3.8 for P_o^{sat}.

Starting with 2.18, substitution of the augmented relationships for the rates of change of oxidizer gas and oxidizer liquid, equations 3.2 and 3.3 obtains:

$$\begin{aligned}
&-P_o^{sat}\hat{V}_{o,l}(-\zeta\dot{n}_{o,f} + \dot{n}_{o,v}) + (V_T - n_{o,l}\hat{V}_{o,l})\frac{dP_o^{sat}}{dT}\dot{T}_T \\
&\qquad = R(T_T(-\zeta\dot{n}_{o,f} + \dot{n}_{o,v}) + n_{o,g}\dot{T}_T) && (3.15)
\end{aligned}$$

Solving for the evaporation rate of nitrous oxide yields:

$$\dot{n}_{o,v} = \left[\frac{b_1}{b_{2,P_o^{sat}}}\right]\dot{T}_T + \left[\frac{(1-\zeta)P_o^{sat}\hat{V}_{o,l} + \zeta RT_T}{b_{2,P_o^{sat}}}\right]\dot{n}_{o,f} \tag{3.16}$$

$$\dot{n}_{o,v} = \left[\frac{b_1}{b_{2,P_o^{sat}}}\right]\dot{T}_T + \left[\frac{(P_o^{sat}\hat{V}_{o,l} + \zeta\left(RT_T - P_o^{sat}\hat{V}_{o,l}\right)}{b_{2,P_o^{sat}}}\right]\dot{n}_{o,f} \tag{3.17}$$

The total pressure of the system is substituted in place of the nitrous oxide saturation pressure. This is done through Raoults law and equation 3.8.

$$\dot{n}_{o,v} = \left[\frac{b_1}{b_{2,P_T}}\right]\dot{T}_T + \left[\frac{\left(\frac{n_{o,g}}{n_{o,g}+n_{He}}\right)P_T\hat{V}_{o,l} + \zeta\left(RT_T - \left(\frac{n_{o,g}}{n_{o,g}+n_{He}}\right)P_T\hat{V}_{o,l}\right)}{b_{2,P_T}}\right]\dot{n}_{o,f} \tag{3.18}$$

$$\dot{n}_{o,v} = \left[\frac{b_1}{b_{2,P_T}}\right]\dot{T}_T + \left[\frac{b_5}{b_{2,P_T}}\right]\dot{n}_{o,f} \tag{3.19}$$

The last remaining relationship required to describe the modified model is the rate of temperature change. Equation 2.21 is taken as the starting point, and equations 3.2 and 3.3 are substituted for the rates of change of the oxidizer liquid and gas phases. This is shown in the following equation.

$$\dot{T}_T = \frac{1}{b_4}(RT_T - \Delta\hat{H}_o)\left[-\zeta\dot{n}_{o,f} + \dot{n}_{o,v}\right] + (P_T\hat{V}_{o,l})\left[-(1-\zeta)\dot{n}_{o,f} - \dot{n}_{o,v}\right] \tag{3.20}$$

Rearrange into terms of total oxidizer outflow and evaporation:

$$\dot{T}_T = \frac{1}{b_4}\left[-\zeta(b_3) - P_T\hat{V}_{o,l}\right]\dot{n}_{o,f} - [b_3]\,\dot{n}_{o,v} \tag{3.21}$$

Equation 3.16 for evaporation rate is substituted into equation 3.21 and then rearranged so the rate of temperature change is described entirely by oxidizer outflow:

$$\dot{T}_T = \left[\frac{\left(\frac{RT_Tn_{He} + \Delta\hat{H}_on_{o,g}}{n_{o,g}+n_{He}}\right)P_T\hat{V}_{o,l}}{b_{2,P_T}b_4 + b_1b_3}\right]\dot{n}_{o,f} \tag{3.22}$$

3.1.4 Implementation of the Model

The model is run in discrete time steps in contrast to the original ideal gas model which is run using an ODE solver. The discrete time step size is 0.002s and is set by the data collection period of the data acquisition system used to collect the results. The pressure in the combustion chamber measurements are directly used in the simulation in contrast to the polynomial equations used in the original ideal gas models.

3.1.5 Optimization of Delay τ and Mixture Ratio ζ

The values for τ and ζ are optimized by using a design of experiments methodology implemented in software [24]. The procedure of optimization is described:

1. Initial values for τ and ζ are selected by estimation.
2. The values for τ and ζ are constrained to be real, positive values. The maximum possible value for τ certainly cannot be longer than the simulation time; the maximum value for ζ is one.
3. High and low values for τ and ζ are determined by varying the original estimates $\pm 20\%$.
4. The simulation is run using all combinations of high and low τ and ζ values, and once using the original estimates.
5. Each iteration of the simulation is evaluated using the following function if the simulation is being optimized for an accurate oxidizer mass simulation:

$$W_{m,\tau,\zeta} = \sum_{k=0}^{t_f} \left(m_{d,k} - m_{s,k}\right)^2 \tag{3.23}$$

where:

- $W_{m,\tau,\zeta}$ is used as a total error value for a specific iteration of the simulation using a combination of τ and ζ values
- $m_{d,k}$ is the mass of remaining oxidizer measured at a specific time point k in the test data

- $m_{s,k}$ is the mass of remaining oxidizer estimated by the simulation at a specific time point k
- t_f is the final time point of the simulation

Or the variables τ and ζ can be optimized for an accurate tank pressure simulation:

$$W_{P_T,\tau,\zeta} = \sum_{k=0}^{t_f} \left(P_{T,d,k} - P_{T,s,k}\right)^2 \tag{3.24}$$

where:

- $W_{P_T,\tau,\zeta}$ is used as a total error value for a specific iteration of the simulation using a combination of τ and ζ values
- $P_{T,d,k}$ is the pressure in the oxidizer tank measured at a specific time point k in the test data
- $P_{T,s,k}$ is the pressure in the oxidizer tank estimated by the simulation at a specific time point k

6. The values p_1, p_2, p_3, p_4, p_5, and p_6 are determined for the following function:

$$W = p_1 + p_2\tau + p_3\zeta + p_4\tau^2 + p_5\tau\zeta + p_6\zeta^2 \tag{3.25}$$

7. The values of τ and ζ that minimize W, the total error, are then determined.
8. If the original estimates and the optimal values of τ and ζ are different by more than 1%, the process is repeated substituting the optimal values of τ and ζ and the estimated original values, or zero, if the estimated optimized values are negative.
9. This process is repeated until the original estimated values of τ and ζ and the optimal values are in agreement to within 1%.

This procedure can be run to optimize τ and ζ for modeling either the mass history or the pressure history. The results of the Case 2 simulation are shown where τ and ζ are optimized to minimize the mass history error. The following figures demonstrate the inability of the modified model to simulate both the mass outflow and the pressure outflow simultaneously. In figure 3.2, the model modifications are shown to increase the accuracy of the simulated mass compared to the original model.

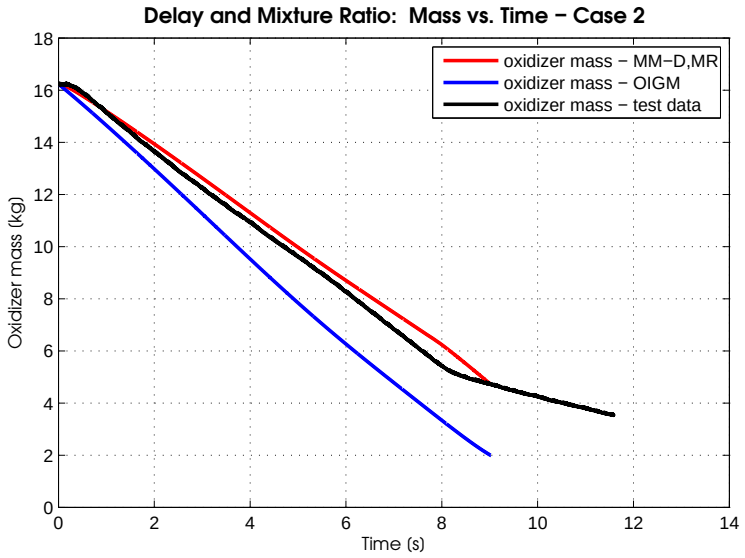

Figure 3.2: Oxidizer mass - Case 2: comparison of Modified Model with Delay and Mixture Ratio (MM-D,MR), Original Ideal Gas Model (OIGM), and testing results

However, figure 3.3 shows this model has reduced accuracy in modeling the tank pressure compared to the original model.

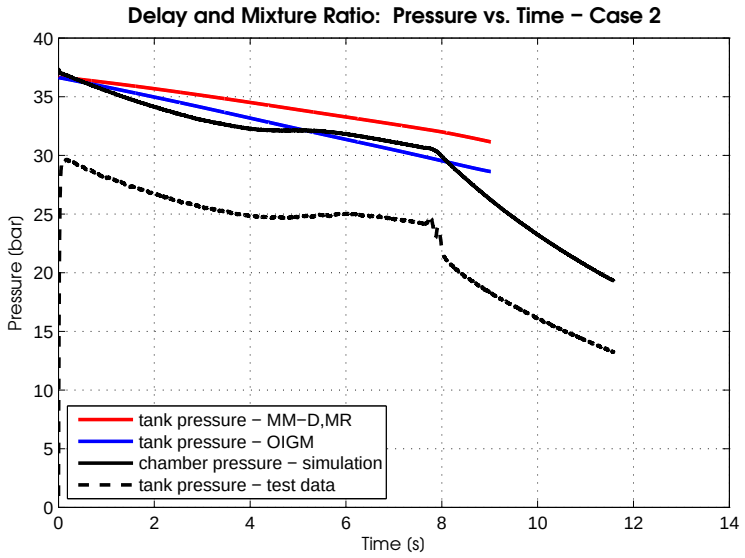

Figure 3.3: Pressure in oxidizer tank - Case 2: comparison of Modified Model with Delay and Mixture Ratio (MM-D,MR), Original Ideal Gas Model (OIGM), and testing results

Figure 3.4 shows that the difference between the saturation temperature and the simulated temperature.

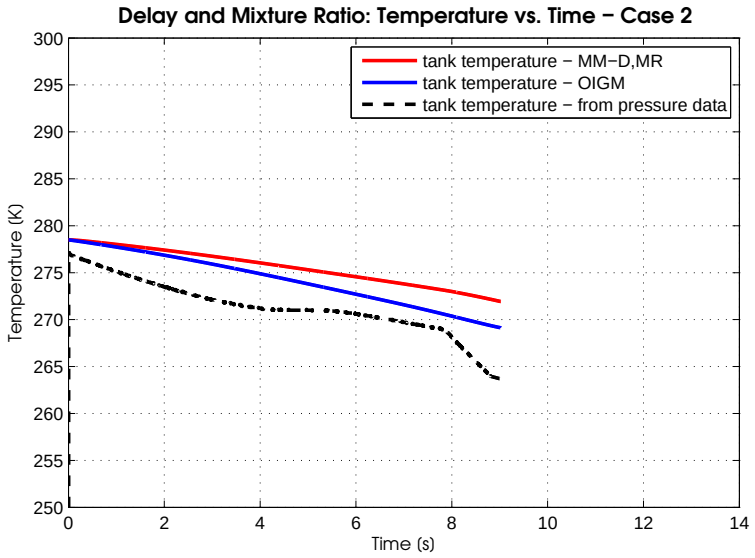

Figure 3.4: Oxidizer temperature - Case 2: comparison of Modified Model with Delay and Mixture Ratio (MM-D,MR), and Original Ideal Gas Model (OIGM) estimations assuming saturation pressure

This indicates that a further modification to the model should be made that allows the system temperature to change more rapidly. It is critical that the model be capable of accurately simulating the mass and pressure of the system. This is because the Extended Kalman Filter oxidizer mass estimate is based on the pressure measurement and the model. Therefore, it is necessary to further refine the model, and a further modification is defined in the next section.

3.2 Ideal Gas Modified Model - Delay, Mixture Ratio and Tank Thermal Mass

The simulated oxidizer tank pressure is based on the saturation pressure of nitrous oxide. The simulated pressure is shown to be higher than the measured pressure in the previous section. In order to reduce the simulated oxidizer pressure, the simulated system temperature must be lower. In order for the model to simulate a system with a temperature decreasing rapidly enough to accurately model the pressure, the thermal mass of the system is reduced. Reducing the thermal mass of the modeled system yields a model with

increased accuracy in mass history and pressure history. This is accomplished in a second version of the modified ideal gas model by removing the thermal mass of oxidizer tank from the system. The assumption that the thermal energy of the oxidizer tank can be neglected is previously used in [15].

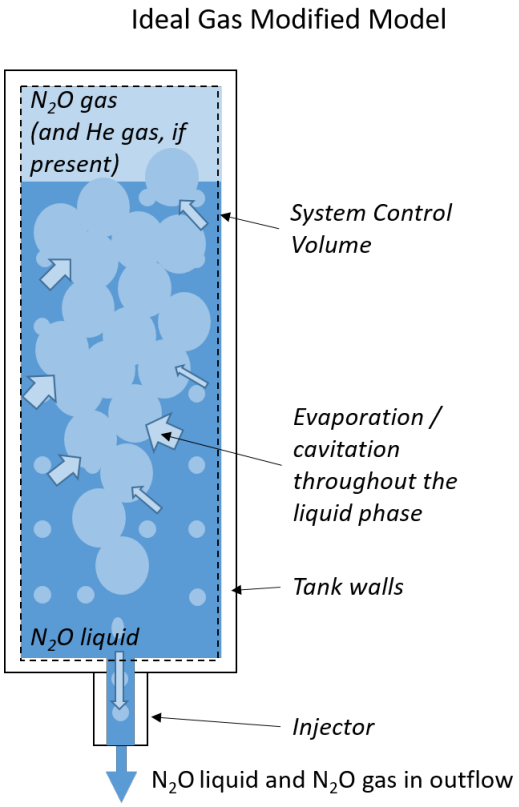

Figure 3.5: Pictorial description of the assumptions made in the second version of the Modified Ideal Gas Model where the thermal mass of the oxidizer tank is removed

The only change from the first version of the Modified Ideal Gas Model to the second version is the assumption that the thermal mass of the oxidizer tank does not significantly interact with the system as nitrous oxide rapidly drains. While in reality an oxidizer tank does reduce in temperature during a test, it does so on a much slower time scale than the fluid inside the tank.

This change in assumptions is easily implemented by changing equation 3.14 to the

following version:

$$b_4 = n_{o,l}\hat{C}_{Vo,l} + n_{o,g}\hat{C}_{Vo,g} + n_{He}\hat{C}_{V,He} \tag{3.26}$$

The values for τ and ζ are optimized using the design of experiment procedure described previously. This procedure is used to optimize the model for both the mass history and pressure history separately. The results of the model optimized for mass and pressure histories are shown for Case 2 only.

First, the results of the model optimized for the mass history are shown in figures 3.6 and 3.7.

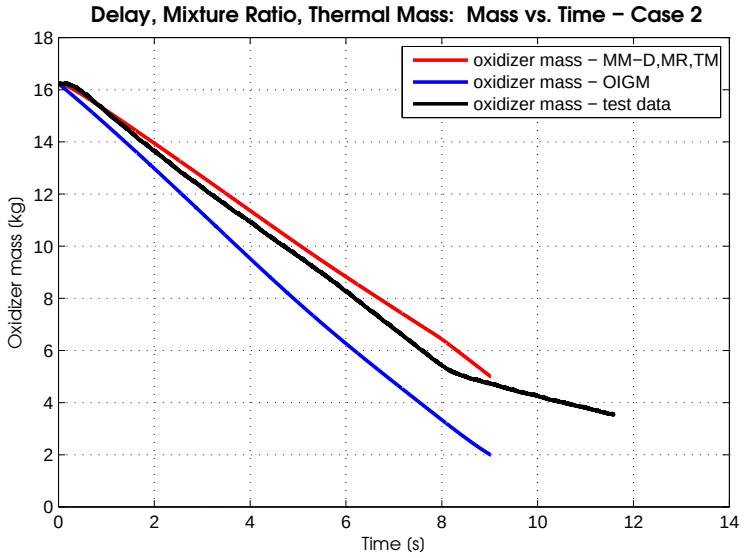

Figure 3.6: Oxidizer mass history - Case 2: comparison of Modified Model with Delay, Mixture Ratio and oxidizer tank Thermal Mass removed(MM-D,MR,TM), Original Ideal Gas Model (OIGM), and testing results; the model is optimized to reduce the error in the mass history

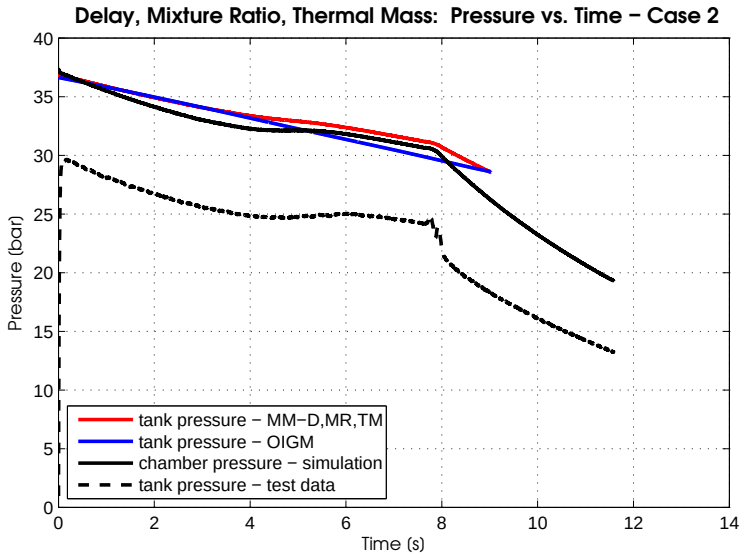

Figure 3.7: Pressure in oxidizer tank - Case 2: comparison of Modified Model with Delay, Mixture Ratio and oxidizer tank Thermal Mass removed(MM-D,MR,TM), Original Ideal Gas Model (OIGM), and testing results; the model is optimized to reduce the error of the mass history

The results of the model optimized for the pressure history are shown in figures 3.8 and 3.9.

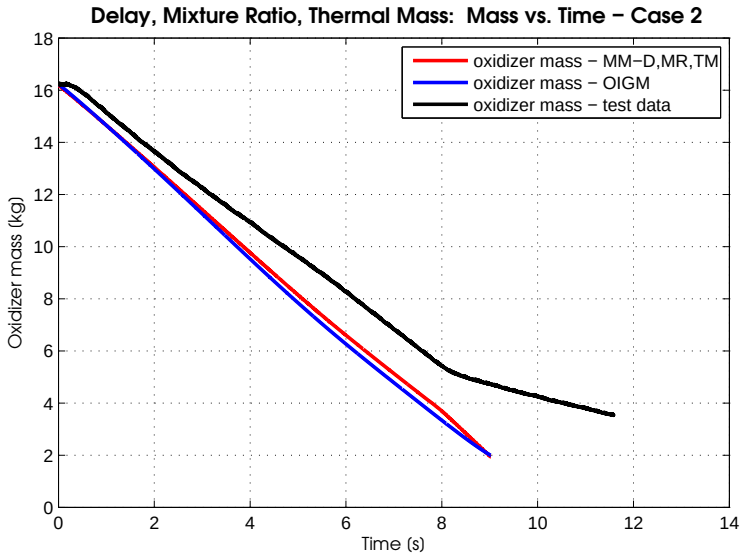

Figure 3.8: Oxidizer mass - Case 2: comparison of Modified Model with Delay, Mixture Ratio and oxidizer tank Thermal Mass removed(MM-D,MR,TM), Original Ideal Gas Model (OIGM), and testing results; the simulation is optimized to minimize the error of the pressure history

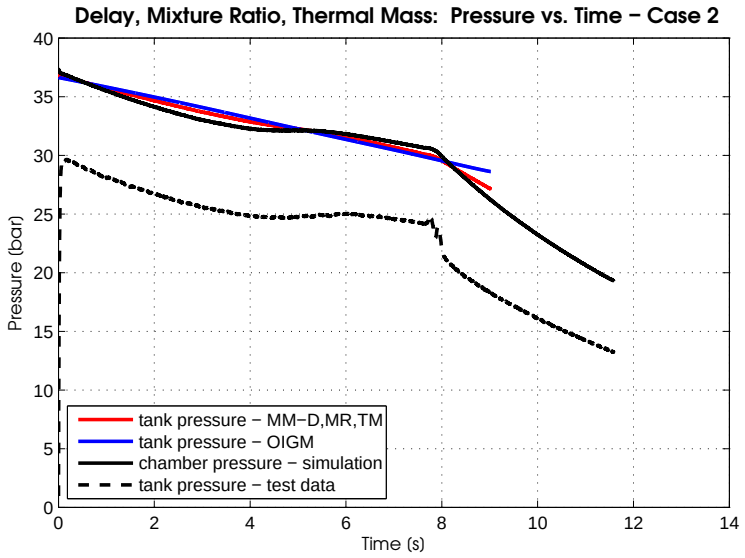

Figure 3.9: Pressure in oxidizer tank - Case 2: comparison of Modified Model with Delay, Mixture Ratio and oxidizer tank Thermal Mass removed(MM-D,MR,TM), Original Ideal Gas Model (OIGM), and testing results; the model is optimized to minimize the error of the pressure history

A summary of the optimized τ and ζ results are shown in the following table.

Data Set	**Optimized State**	**Optimal Delay τ [s]**	**Optimal Mixture Ratio ζ [–]**
Case 2	mass	0.1486	0.3944
	pressure	0.0003	0.0516
Case 3	mass	0.2844	0.3659
	pressure	0.0005	0.2090
Average		0.1085	0.2552

Table 3.1: Summary of optimized τ and ζ values

Optimized values for τ and ζ vary significantly when the error is reduced between the pressure history and the mass history. This variation highlights that dynamics that exist in the real system are not taken into account in the model. The optimal values for τ are larger when the model is optimized for mass accuracy rather than for pressure accuracy;

this merely indicates that the delay is more clearly observed in the mass test data than the pressure test data. The optimized ζ values also vary significantly between the mass and pressure accuracy optimization, and through the two test data cases. This indicates that a fixed mixture ratio may over simplify the model if increased accuracy is desired. There is also variability between the optimized values for Case 2 and Case 3. This indicates that the values for τ and ζ may depend on the initial conditions of the system being tested; however, two data sets are not sufficient to draw any conclusions about the potential links between the initial conditions are the optimized values. However simplified, the model is developed with the goal of predicting the mass of oxidizer in a tank during flight. In the next chapter, it is determined if this model is sufficiently detailed for this purpose.

3.3 Discussion of Modified Model Results

This section contains the results of the modified ideal gas model in its second version. The values for τ and ζ that are applied are the averages that are shown in table 3.1. The results are compared to the data of the two test cases, and to the original ideal gas model. The modified ideal gas model does not describe all the dynamics of the real system. This is observed in the results; however, the following figures do show that the modified model is capable to better simulate the actual systems mass history.

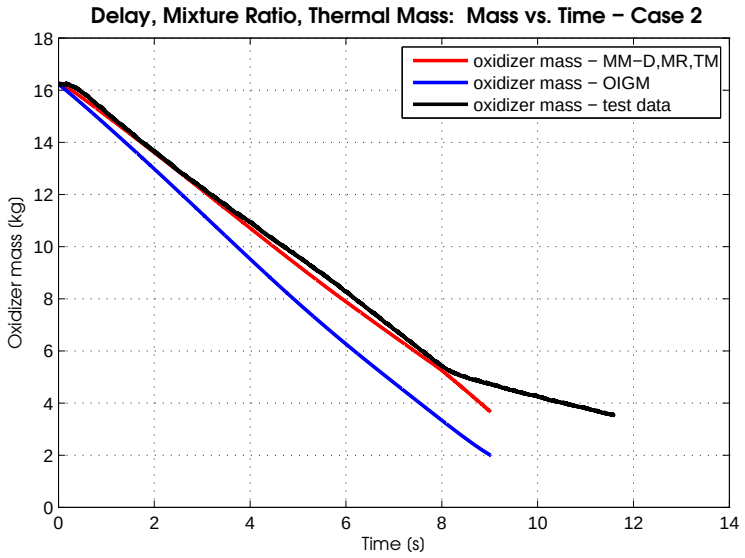

Figure 3.10: Oxidizer mass - Case 2: comparison of Modified Model with Delay, Mixture Ratio and oxidizer tank Thermal Mass removed(MM-D,MR,TM), Original Ideal Gas Model (OIGM), and testing results

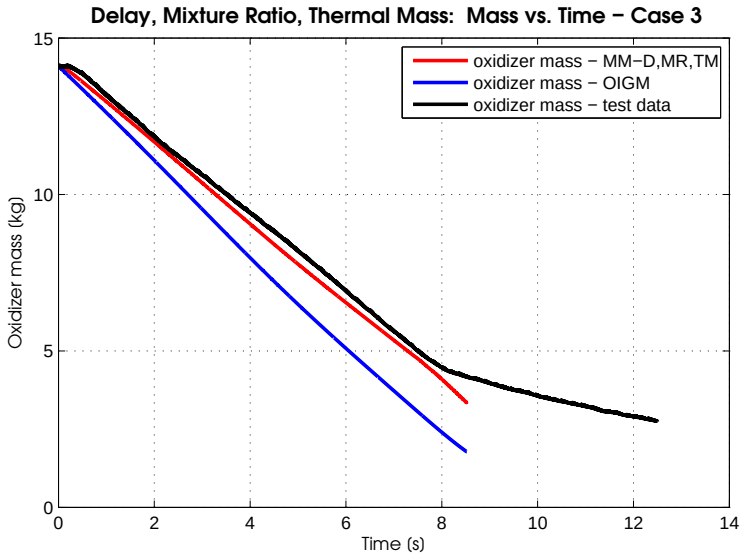

Figure 3.11: Oxidizer mass - Case 3: comparison of Modified Model with Delay, Mixture Ratio and oxidizer tank Thermal Mass removed(MM-D,MR,TM), Original Ideal Gas Model (OIGM), and testing results

The modified ideal gas model also does not describe the additional dynamics observed in the real system. The measured pressure fluctuates to values both greater and less than the simulation. In [17], it is shown that these events correlate with the boiling of the oxidizer. Initially, a transient form of boiling takes place as the rate of bubble development exceeds the rate of bubbles entering the ullage. This occurs during the initial loss of pressure. Boiling then develops a steady state as the rate of bubble development and the loss of bubbles to the ullage reaches a steady state. These dynamics are not accounted for in the model modifications in this thesis. At approximately the 8 second mark of the data collected for both Case 2 and Case 3, there is a steep drop-off of pressure measured in the actual system. This is usually considered to be the point where all remaining nitrous oxide is in the gas phase. In future graphs, it is shown that the modified model predicts the presence of liquid nitrous oxide even after this distinct drop-off of pressure.

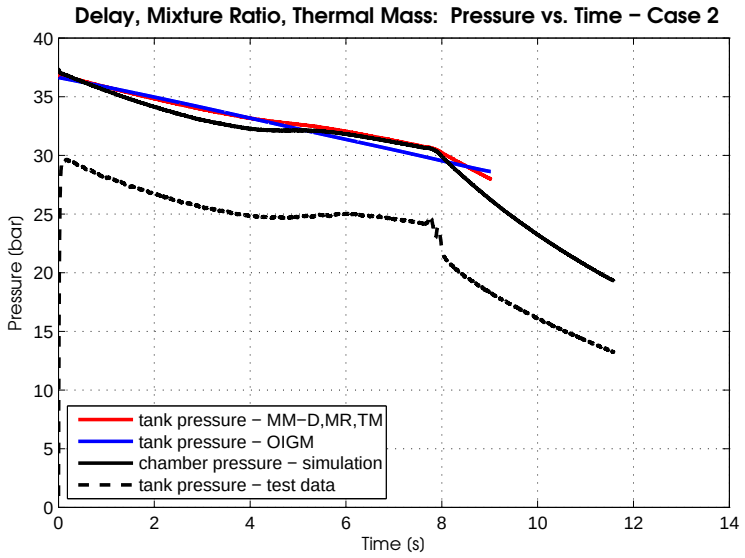

Figure 3.12: Pressure in oxidizer tank - Case 2: comparison of Modified Model with Delay, Mixture Ratio and oxidizer tank Thermal Mass removed(MM-D,MR,TM), Original Ideal Gas Model (OIGM), and testing results; the model compromises between low error in both mass and pressure histories

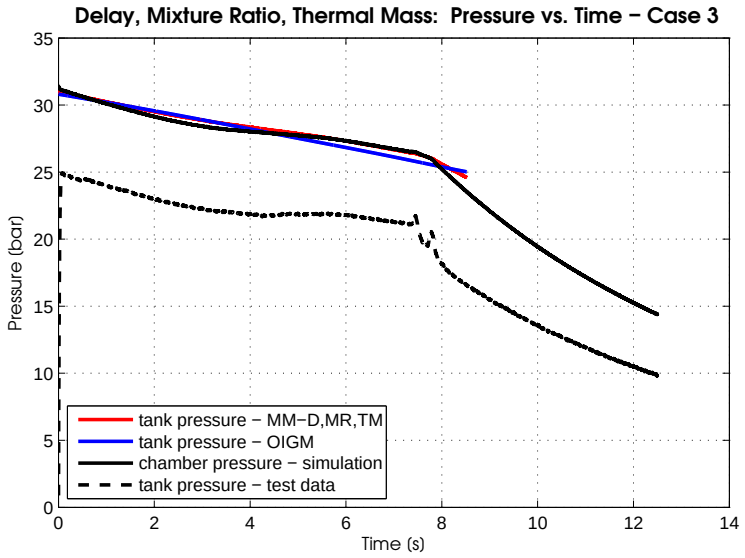

Figure 3.13: Pressure in oxidizer tank - Case 3: comparison of Modified Model with Delay, Mixture Ratio and oxidizer tank Thermal Mass removed(MM-D,MR,TM), Original Ideal Gas Model (OIGM), and testing results; the model compromises between low error in both mass and pressure histories

It is difficult to discern a significant difference in the temperatures estimated by the models. The subtle differences in temperature are more prominent in the differences of tank pressures shown in the previous figures.

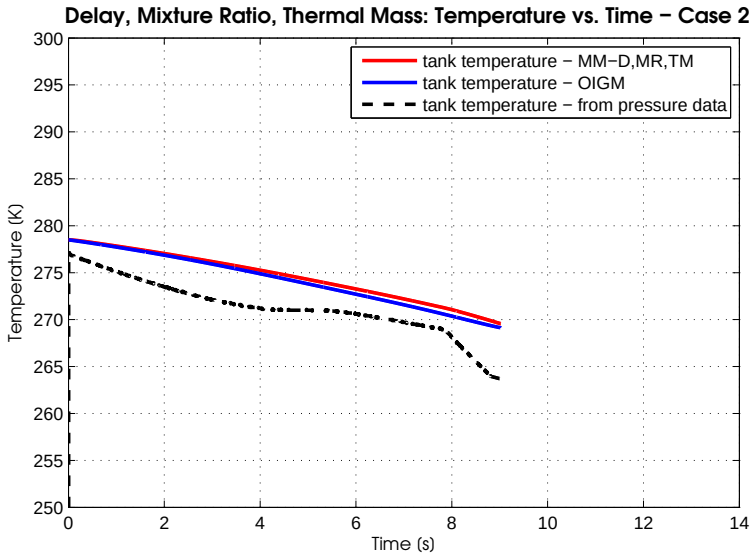

Figure 3.14: Oxidizer temperature - Case 2: comparison of Modified Model with Delay, Mixture Ratio and oxidizer tank Thermal Mass removed(MM-D,MR,TM) and Original Ideal Gas Model (OIGM) estimations assuming saturation pressure; the model compromises between low error in both mass and pressure histories

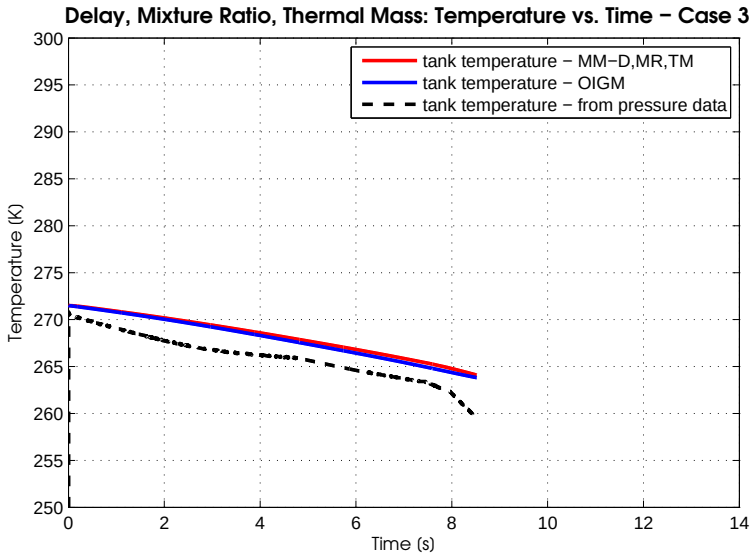

Figure 3.15: Oxidizer temperature - Case 3: comparison of Modified Model with Delay, Mixture Ratio and oxidizer tank Thermal Mass removed(MM-D,MR,TM) and Original Ideal Gas Model (OIGM) estimations assuming saturation pressure; the model compromises between low error in both mass and pressure histories

The modified models predict that there are still liquid nitrous oxide moles present in the system after the original model predicts that all moles in the tank are in the gas phase. This results from the assumption that less liquid moles are flowing through the injector in the modified model.

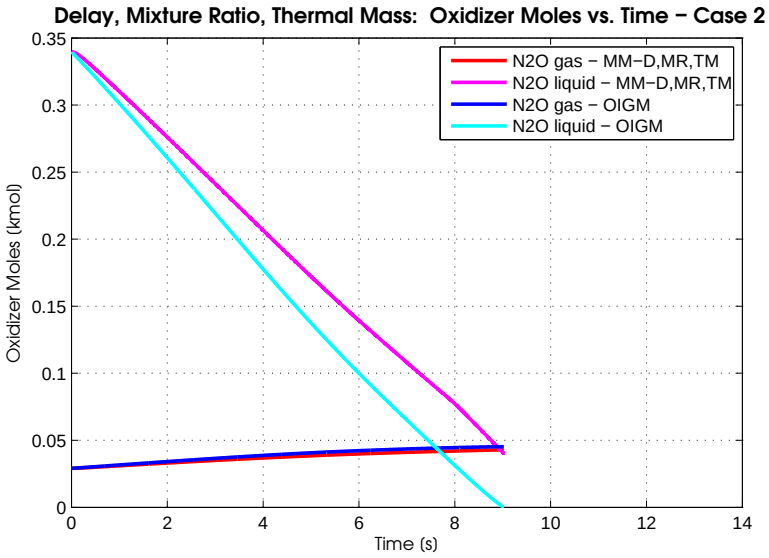

Figure 3.16: Moles of oxidizer phases - Case 2: comparison of Modified Model with Delay, Mixture Ratio and oxidizer tank Thermal Mass removed(MM-D,MR,TM) and Original Ideal Gas Model (OIGM) estimations

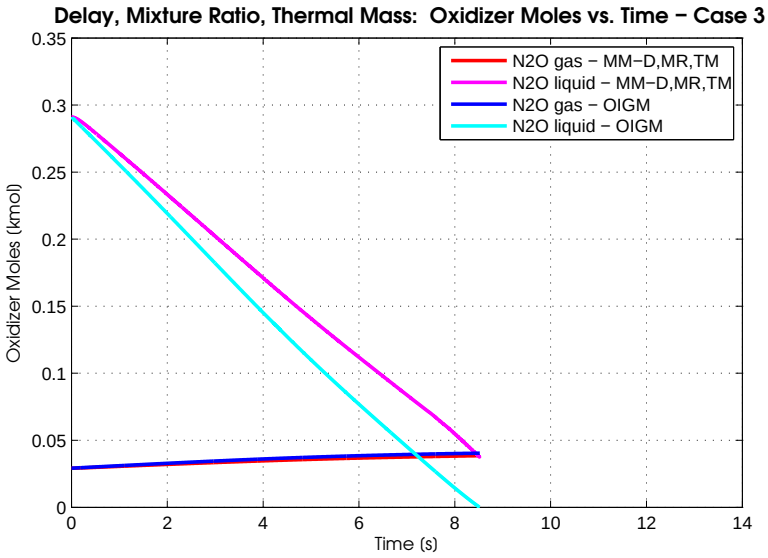

Figure 3.17: Moles of oxidizer phases - Case 3: comparison of Modified Model with Delay, Mixture Ratio and oxidizer tank Thermal Mass removed(MM-D,MR,TM) and Original Ideal Gas Model (OIGM) estimations

The estimates of the nitrous oxide outflow temperature show a better average agreement with reality; however, it is obvious that trends that exist in reality are not present in the modified model.

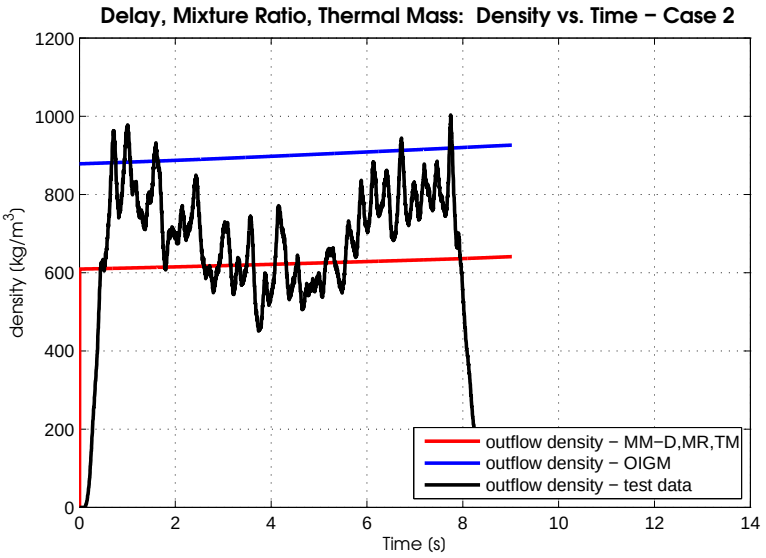

Figure 3.18: Oxidizer outflow density - Case 2: comparison of Modified Model with Delay, Mixture Ratio and oxidizer tank Thermal Mass removed(MM-D,MR,TM) and Original Ideal Gas Model (OIGM) estimations

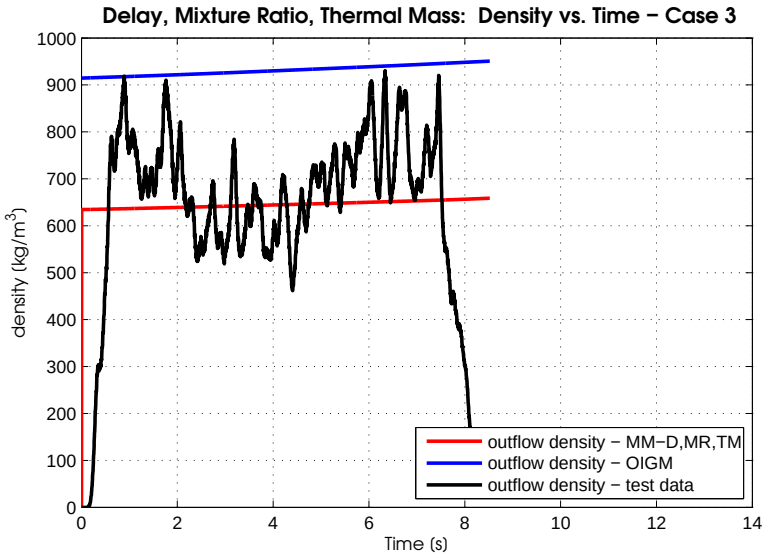

Figure 3.19: Oxidizer outflow density - Case 3: comparison of Modified Model with Delay, Mixture Ratio and oxidizer tank Thermal Mass removed(MM-D,MR,TM) and Original Ideal Gas Model (OIGM) estimations

The modified model more closely unites the pressure history and the mass history of the real system than the original model. It is still obvious that the modified model omits system dynamics that are present in reality, specifically a detailed model of boiling. Next, the modified model is applied in an Extended Kalman Filter that can be used to dynamically estimate the remaining nitrous oxide mass by using known initial conditions and measuring the pressure of the oxidizer tank.

Chapter 4

Derivation of Extended Kalman Filter

This section describes the structure of the Extended Kalman Filter developed for estimating the remaining mass of nitrous oxide remaining in an oxidizer tank. This filter uses the oxidizer outflow model that has been developed in the previous chapter. The filter is developed in discrete time. The states are described in the previous chapter and maintained in this use of the model with discrete time notation added:

$$x_k = \begin{bmatrix} (m_o)_k \\ (P_T)_k \\ (T_T)_k \\ (\dot{T}_T)_k \\ (n_{o,l})_k \\ (n_{o,g})_k \end{bmatrix} \tag{4.1}$$

where x_k refers to the vector of states at a discrete time step and the subscript k refers to a specific time step.

The control inputs are:

$$u_k = \begin{bmatrix} (C_D A_{inj})_k \\ (P_C)_k \end{bmatrix} \tag{4.2}$$

where u_k refers to the control vector at a discrete time step. The cross sectional area of the injector A_{inj} and the flow coefficient C_d are combined intentionally. This allows the flow rate to be controlled by changing the area or the flow coefficient geometry.

The measurement input is:

$$y_k = \begin{bmatrix} (P_T)_k \end{bmatrix} \tag{4.3}$$

where y_k refers to the measurement vector at a discrete time step. Pressure is the only measurement included in order to evaluate the Extended Kalman Filter's accuracy with minimal sensors. In other oxidizer tank designs it may be possible to include a temperature sensor; however, temperature data is not available with the provided test results.

4.1 Initializing the System States

This section describes how the states in 4.1 are initialized. The states that are implemented through a direct measurement are summarized below:

- Initial mass of oxidizer $(m_o)_0$ is measured and provided to the filter at launch time.
- Initial oxidizer tank pressure $(P_T)_0$ is the measurement at the initial time point; oxidizer tank pressure is measured continuously.
- Initial oxidizer temperature $(T_T)_0$ is assumed to be equal to the temperature of the surrounding environment and can be provided to the filter at launch time.
- Initial rate of oxidizer temperature change $(\dot{T}_T)_0$ is assumed to be zero or negligible.
- Initial molar amounts of gas and liquid phase nitrous oxide are determined using the measurements and assumptions above and the equations below:

$$(n_{o,l})_0 = \frac{\frac{(m_o)_0}{M_o} R(T_T)_0 - P_o^{sat} V_T}{-P_o^{sat} \hat{V}_{o,l} + R(T_T)_0} \tag{4.4}$$

$$(n_{o,g})_0 = \frac{P_o^{sat}(V_T - \hat{V}_{o,l} \frac{(m_o)_0}{M_o})}{-P_o^{sat} \hat{V}_{o,l} + R(T_T)_0} \tag{4.5}$$

The system is assumed to be at the same temperature as the surrounding environment prior to launch. The temperature is assumed to be constant; therefore the initial rate of temperature change is assumed to be zero initially. The number of moles of nitrous oxide

in the liquid and gas phases can be determined by assuming the entire mass of nitrous oxide is at equilibrium. These initial conditions are summarized in the equations below.

$$(m_o)_0 = m_{o,0} \tag{4.6}$$
$$(P_T)_0 = P_0 \tag{4.7}$$
$$(T_T)_0 = T_0 \tag{4.8}$$
$$(\dot{T}_T)_0 = 0 \tag{4.9}$$
$$(n_{o,l})_0 = \frac{\frac{(m_o)_0}{M_o} R(T_T)_0 - P_o^{sat} V_T}{-P_o^{sat} \hat{V}_{o,l} + R(T_T)_0} \tag{4.10}$$
$$(n_{o,g})_0 = \frac{P_o^{sat}(V_T - \hat{V}_{o,l} \frac{(m_o)_0}{M_o})}{-P_o^{sat} \hat{V}_{o,l} + R(T_T)_0} \tag{4.11}$$

These functions are referred to as f, and this notation is used later in equation 4.74.

4.2 System Model

The following procedure is followed at each discrete time step of the Extended Kalman Filter's operation.

4.2.1 Nitrous Oxide Equilibrium Properties

The first step in the system model is to determine the saturation properties of nitrous oxide as a functions of temperature:

$$P_o^{sat} = g_1((T_T)_{k-1}) \tag{4.12}$$
$$\hat{V}_{o,l} = g_2((T_T)_{k-1}) \tag{4.13}$$
$$\hat{C}_{o,l} = g_3((T_T)_{k-1}) \tag{4.14}$$
$$\hat{C}_{o,g} = g_4((T_T)_{k-1}) \tag{4.15}$$
$$\frac{dP_o^{sat}}{dT} = g_5((T_T)_{k-1}) \tag{4.16}$$

where g_x refers to the use of a function.

4.2.2 Nitrous Oxide Outflow Rate and Evaporation Rate

The second step in the system model is to determine the rate of oxidizer outflow from the tank and the rate of oxidizer evaporation within the tank.

$$(\rho_f)_k = \zeta \frac{(P_T)_{k-1}}{R(T_T)_{k-1}} + (1-\zeta)\frac{1}{\hat{V}_{o,l}} \tag{4.17}$$

$$(\Delta P)_k = ((P_T)_{k-1} - (P_C)_k) \tag{4.18}$$

$$(\dot{n}_{o,f})_k = (C_D A_{inj})_k \sqrt{\left(\frac{2}{M_o}\right)(\rho_f)_k (\Delta P)_k}\left(1 - \exp\left(\frac{-dtk}{\tau}\right)\right) \tag{4.19}$$

The following terms are defined in order to facilitate the display of equations for evaporation rate and rate of temperature change:

$$(b_1)_k = (V_T - (n_{o,l})_{k-1}\hat{V}_{o,l})\frac{dP_o^{sat}}{dT} - R(n_{o,g})_{k-1} \tag{4.20}$$

$$(b_{2,P_T})_k = R(T_T)_{k-1} - \left(\frac{(n_{o,g})_{k-1}}{(n_{o,g})_{k-1} + n_{He}}\right)(P_T)_{k-1}\hat{V}_{o,l} \tag{4.21}$$

$$(b_3)_k = (P_T)_{k-1}\hat{V}_{o,l} - R(T_T)_{k-1} + \Delta\hat{H}_o \tag{4.22}$$

$$(b_4)_k = (n_{o,l})_{k-1}\hat{C}_{Vo,l} + (n_{o,g})_{k-1}\hat{C}_{Vo,g} + n_{He}\hat{C}_{V,He} \tag{4.23}$$

$$(b_5)_k = \left(\frac{(n_{o,g})_{k-1}}{(n_{o,g})_{k-1} + n_{He}}\right)(P_T)_{k-1}\hat{V}_{o,l} + \zeta(b_{2,P_T})_k \tag{4.24}$$

$$(b_6)_k = \left(\frac{-R(T_T)_{k-1} - \Delta\hat{H}_o(n_{o,g})_{k-1}}{(n_{o,g})_{k-1} + n_{He}}\right)(P_T)_{k-1}\hat{V}_{o,l} \tag{4.25}$$

Given the previous definitions, the rate of nitrous oxide evaporation is represented in the following equation.

$$\dot{n}_{o,v} = \left[\frac{(b_1)_k}{(b_{2,P_T})_k}\right](\dot{T}_T)_k + \left[\frac{(b_5)_k}{(b_{2,P_T})_k}\right](\dot{n}_{o,f})_k \tag{4.26}$$

4.2.3 State Updates

The following equations follow directly from the derivation of the ideal gas modified model with the injector delay τ, mixture ratio ζ and removal of the oxidizer tank's thermal mass

from the system. Many terms have partial derivatives that go to zero; these are not shown.

$$
\begin{aligned}
(m_o)_k &= M_o * [(n_{o,l})_{k-1} + (n_{o,g})_{k-1} - dt * (\dot{n}_{o,f})_k] && (4.27)\\
(P_T)_k &= \frac{(n_{o,g})_{k-1} + n_{He}}{(n_{o,g})_{k-1}} P_{o_k}^{sat} && (4.28)\\
(T_T)_k &= (T_T)_{k-1} + dt * (\dot{T}_T)_{k-1} && (4.29)\\
(\dot{T}_T)_k &= \left[\frac{(b_6)_k}{(b_{2,P_{T_k}})(b_4)_k + (b_1)_k (b_3)_k} \right] \dot{n}_{o,f_k} && (4.30)\\
(n_{o,l})_k &= (n_{o,l})_{k-1} - dt\,[(1-\zeta)(\dot{n}_{o,f})_k + (\dot{n}_{o,v})_k] && (4.31)\\
(n_{o,g})_k &= (n_{o,g})_{k-1} - dt\,[\zeta(\dot{n}_{o,f})_k - (\dot{n}_{o,v})_k] && (4.32)
\end{aligned}
$$

where dt refers to the discrete amount of time between time points in the filter.

4.3 Jacobian of the System Model

The next step in the development of the Extended Kalman Filter is to determine the partial derivatives of the system model with respect to the system states. The partial derivatives are developed once, then updated every time step.

4.3.1 Partial Derivatives of Mass Outflow Rate

The partial derivatives for mass outflow rate are used multiple times, they are derived here first and referred to later. Note that the first order delay term is not used in partial derivatives.

$$
\left(\frac{\partial \dot{n}_{o,f}}{\partial P_T} \right)_k = (C_D A_{inj})_k \left(\frac{[2(P_T)_{k-1} - (P_C)_k] \left(\frac{\zeta}{R(T_T)_{k-1}} \right) + \frac{1-\zeta}{\hat{V}_{o,l}}}{M_o \sqrt{(\rho_f)_k (\Delta P)_k}} \right) \quad (4.33)
$$

$$
\left(\frac{\partial \dot{n}_{o,f}}{\partial T_T} \right)_k = (C_D A_{inj})_k \left(\frac{[(P_T)_{k-1} - (P_C)_k] \left(\frac{-\zeta}{R(T_T)_{k-1}^2} + \frac{1-\zeta}{\hat{V}_{o,l}} \right)}{M_o \sqrt{(\rho_f)_k (\Delta P)_k}} \right) \quad (4.34)
$$

4.3.2 Partial Derivatives of Oxidizer Evaporation Rate

The partial derivatives for nitrous oxide evaporation rate are shown here and referred to in the partial derivatives for other system functions. The partial derivatives of terms $(b_1)_k$, $(b_{2,P_T})_k$, $(b_3)_k$, $(b_4)_k$, $(b_5)_k$ and $(b_6)_k$ are taken individually, then pieced back together as appropriate and as needed. Partial derivatives with respect to tank pressure:

$$\left(\frac{\partial b_{2,P_T}}{\partial P_T}\right)_k = -\left(\frac{(n_{o,g})_{k-1}}{(n_{o,g})_{k-1}+n_{He}}\right)\hat{V}_{o,l} \tag{4.35}$$

$$\left(\frac{\partial b_3}{\partial P_T}\right)_k = \hat{V}_{o,l} \tag{4.36}$$

$$\left(\frac{\partial b_5}{\partial P_T}\right)_k = \left((\zeta-1)\frac{(n_{o,g})_{k-1}}{(n_{o,g})_{k-1}+n_{He}}\right)\hat{V}_{o,l} \tag{4.37}$$

$$\left(\frac{\partial b_6}{\partial P_T}\right)_k = \left(\frac{\Delta\hat{H}_o - R(T_T)_{k-1}}{((n_{o,g})_{k-1}+n_{He})^2}\right)\hat{V}_{o,l} \tag{4.38}$$

Partial derivatives with respect to tank temperature:

$$\left(\frac{\partial b_{2,P_T}}{\partial T_T}\right)_k = R \tag{4.39}$$

$$\left(\frac{\partial b_3}{\partial T_T}\right)_k = -R \tag{4.40}$$

$$\left(\frac{\partial b_5}{\partial T_T}\right)_k = \zeta R \tag{4.41}$$

$$\left(\frac{\partial b_6}{\partial T_T}\right)_k = \left(\frac{R(P_T)_{k-1}\hat{V}_{o,l}}{(n_{o,g})_{k-1}+n_{He}}\right) \tag{4.42}$$

Partial derivatives with respect to the number of liquid oxidizer moles:

$$\left(\frac{\partial b_1}{\partial n_{o,l}}\right)_k = \hat{V}_{o,l}\frac{dP_o^{sat}}{dT} \tag{4.43}$$

$$\left(\frac{\partial b_4}{\partial n_{o,l}}\right)_k = \hat{C}_{Vo,l} \tag{4.44}$$

Partial derivatives with respect to the number of gas nitrous oxide moles:

$$\left(\frac{\partial b_1}{\partial n_{o,g}}\right)_k = -R \tag{4.45}$$

$$\left(\frac{\partial b_{2,P_T}}{\partial n_{o,g}}\right)_k = -\left(\frac{n_{He}}{(n_{o,g})_{k-1}+n_{He})^2}\right)(P_T)_{k-1}\hat{V}_{o,l} \tag{4.46}$$

$$\left(\frac{\partial b_4}{\partial n_{o,g}}\right)_k = \hat{C}_{Vo,g} \tag{4.47}$$

$$\left(\frac{\partial b_5}{\partial n_{o,g}}\right)_k = (\zeta-1)\left(\frac{n_{He}}{(n_{o,g})_{k-1}+n_{He})^2}\right)(P_T)_{k-1}\hat{V}_{o,l} \tag{4.48}$$

$$\left(\frac{\partial b_6}{\partial n_{o,g}}\right)_k = \left(\frac{\hat{H}_o(n_{o,g})_{k-1}-R(T_T)_{k-1}}{(n_{o,g})_{k-1}+n_{He})^2}\right)(P_T)_{k-1}\hat{V}_{o,l} \tag{4.49}$$

The partial derivatives of the nitrous oxide evaporation rate:

$$\left(\frac{\partial \dot{n}_{o,v}}{\partial P_T}\right)_k = \left[\frac{-(b_1)_k \left(\frac{\partial b_{2,P_T}}{\partial P_T}\right)_k}{(b_{2,P_T})_k^2}\right] (\dot{T}_T)_{k-1} + \left[\frac{\frac{\partial b_5}{\partial P_T}(b_{2,P_T})_k - (b_5)_k \left(\frac{\partial b_{2,P_T}}{\partial P_T}\right)_k}{(b_{2,P_T})_k^2}\right] (\dot{n}_{o,f})_k + \left[\frac{(b_5)_k}{(b_{2,P_T})_k}\right] \frac{\partial \dot{n}_{o,f}}{\partial P_T} \tag{4.50}$$

$$\left(\frac{\partial \dot{n}_{o,v}}{\partial T_T}\right)_k = \left[\frac{-(b_1)_k \left(\frac{\partial b_{2,P_T}}{\partial T_T}\right)_k}{(b_{2,P_T})_k^2}\right] (\dot{T}_T)_{k-1} + \left[\frac{\left(\frac{\partial b_5}{\partial T_T}\right)_k (b_{2,P_T})_k - (b_5)_k \left(\frac{\partial b_{2,P_T}}{\partial T_T}\right)_k}{(b_{2,P_T})_k^2}\right] (\dot{n}_{o,f})_k + \left[\frac{(b_5)_k}{(b_{2,P_T})_k}\right] \left(\frac{\partial \dot{n}_{o,f}}{\partial T_T}\right)_k \tag{4.51}$$

$$\left(\frac{\partial \dot{n}_{o,v}}{\partial \dot{T}_T}\right)_k = \frac{(b_1)_k}{(b_{2,P_T})_k} \tag{4.52}$$

$$\left(\frac{\partial \dot{n}_{o,v}}{\partial n_{o,l}}\right)_k = \left[\frac{\left(\frac{\partial b_1}{\partial n_{o,g}}\right)_k (b_{2,P_T})_k}{(b_{2,P_T})_k^2}\right] (\dot{T}_T)_{k-1} \tag{4.53}$$

$$\begin{aligned}\left(\frac{\partial \dot{n}_{o,v}}{\partial n_{o,g}}\right)_k &= \left[\frac{\left(\frac{\partial b_1}{\partial n_{o,g}}\right)_k (b_{2,P_T})_k - (b_1)_k \left(\frac{\partial b_{2,P_T}}{\partial n_{o,g}}\right)_k}{(b_{2,P_T})_k^2}\right] (\dot{T}_T)_{k-1} \\ &+ \left[\frac{\left(\frac{\partial b_5}{\partial n_{o,g}}\right)_k (b_{2,P_T})_k - (b_5)_k \left(\frac{\partial b_{2,P_T}}{\partial n_{o,g}}\right)_k}{(b_{2,P_T})_k^2}\right] (\dot{n}_{o,f})_k \end{aligned} \tag{4.54}$$

The following partial derivatives are the components of the system Jacobian. The partial derivatives of the nitrous oxide mass are:

$$\left(\frac{\partial m_o}{\partial P_T}\right)_k = -M_o dt \left(\frac{\partial \dot{n}_{o,f}}{\partial P_T}\right)_k \tag{4.55}$$

$$\left(\frac{\partial m_o}{\partial T_T}\right)_k = -M_o dt \left(\frac{\partial \dot{n}_{o,f}}{\partial T_T}\right)_k \tag{4.56}$$

$$\left(\frac{\partial m_o}{\partial n_{o,l}}\right)_k = -M_o \tag{4.57}$$

$$\left(\frac{\partial m_o}{\partial n_{o,g}}\right)_k = -M_o \tag{4.58}$$

The partial derivative of the total tank pressure with respect to the number of nitrous oxide gas moles is:

$$\left(\frac{\partial P_T}{\partial n_{o,g}}\right)_k = \frac{-n_{He}}{(n_{o,g})_{k-1}^2} P_o^{sat} \tag{4.59}$$

The partial derivative of the tank temperature with respect to the rate of temperature range is:

$$\left(\frac{\partial T_T}{\partial \dot{T}_T}\right)_k = dt \tag{4.60}$$

The partial derivatives of the rate of temperature change are:

$$\begin{aligned}
\left(\frac{\partial \dot{T}_T}{\partial P_T}\right)_k &= \left[\frac{\left(\frac{\partial b_6}{\partial P_T}\right)_k}{[(b_{2,P_T})_k(b_4)_k + (b_1)_k(b_3)_k]}\right](\dot{n}_{o,f})_k \\
&- \left[\frac{(b_6)_k\left[\left(\frac{\partial b_{2,P_T}}{\partial P_T}\right)_k(b_4)_k - \left(\frac{\partial b_3}{\partial P_T}\right)_k(b_1)_k\right]}{[(b_{2,P_T})_k(b_4)_k + (b_1)_k(b_3)_k]^2}\right](\dot{n}_{o,f})_k \\
&+ \left[\frac{(b_6)_k}{(b_{2,P_T})_k(b_4)_k + (b_1)_k(b_3)_k}\right]\left(\frac{\partial \dot{n}_{o,f}}{\partial P_T}\right)_k \\
\left(\frac{\partial \dot{T}_T}{\partial T_T}\right)_k &= \left[\frac{\left(\frac{\partial b_6}{\partial T_T}\right)_k}{[(b_{2,P_T})_k(b_4)_k + (b_1)_k(b_3)_k]}\right](\dot{n}_{o,f})_k \\
&- \left[\frac{(b_6)_k\left[\left(\frac{\partial b_{2,P_T}}{\partial T_T}\right)_k(b_4)_k - \left(\frac{\partial (b_3)_k}{\partial T_T}\right)_k(b_1)_k\right]}{[(b_{2,P_T})_k(b_4)_k + (b_1)_k(b_3)_k]^2}\right]\dot{n}_{o,f} \\
&+ \left[\frac{(b_6)_k}{(b_{2,P_T})_k(b_4)_k + (b_1)_k(b_3)_k}\right]\left(\frac{\partial \dot{n}_{o,f}}{\partial T_T}\right)_k \\
\left(\frac{\partial \dot{T}_T}{\partial n_{o,l}}\right)_k &= \left[\frac{-(b_6)_k(b_{2,P_T})_k\left(\frac{\partial b_4}{\partial n_{o,l}}\right)_k + (b_1)_k\left(\frac{\partial b_4}{\partial n_{o,l}}\right)_k}{[(b_{2,P_T})_k(b_4)_k + (b_1)_k(b_3)_k]^2}\right]\dot{n}_{o,f}
\end{aligned} \tag{4.61}$$

$$\begin{aligned}
\left(\frac{\partial \dot{T}_T}{\partial n_{o,g}}\right)_k &= \left[\frac{\left(\frac{\partial b_6}{\partial n_{o,g}}\right)_k}{[(b_{2,P_T})_k(b_4)_k + (b_1)_k(b_3)_k]}\right]\dot{n}_{o,f} \\
- &\left[\frac{(b_6)_k\left[\left(\frac{\partial b_{2,P_T}}{\partial n_{o,g}}\right)_k(b_4)_k + \left(\frac{\partial b_4}{\partial n_{o,g}}\right)_k(b_{2,P_T})_k + \left(\frac{\partial b_1}{\partial n_{o,g}}\right)_k(b_3)_k\right]}{[(b_{2,P_T})_k(b_4)_k + (b_1)_k(b_3)_k]^2}\right]\dot{n}_{o,f}
\end{aligned} \tag{4.62}$$

The partial derivatives of the nitrous oxide liquid moles are:

$$\left(\frac{\partial n_{o,l}}{\partial P_T}\right)_k = -dt\left[(1-\zeta)\left(\frac{\partial \dot{n}_{o,f}}{\partial P_T}\right)_k - \left(\frac{\partial \dot{n}_{o,v}}{\partial P_T}\right)_k\right] \tag{4.63}$$

$$\left(\frac{\partial n_{o,l}}{\partial T_T}\right)_k = -dt\left[(1-\zeta)\left(\frac{\partial \dot{n}_{o,f}}{\partial T_T}\right)_k - \left(\frac{\partial \dot{n}_{o,v}}{\partial T_T}\right)_k\right] \tag{4.64}$$

$$\left(\frac{\partial n_{o,l}}{\partial \dot{T}_T}\right)_k = -dt\left[\left(\frac{\partial \dot{n}_{o,v}}{\partial \dot{T}_T}\right)_k\right] \tag{4.65}$$

$$\left(\frac{\partial n_{o,l}}{\partial n_{o,l}}\right)_k = -dt\left[\left(\frac{\partial \dot{n}_{o,v}}{\partial n_{o,l}}\right)_k\right] \tag{4.66}$$

$$\left(\frac{\partial n_{o,l}}{\partial n_{o,g}}\right)_k = -dt\left[\left(\frac{\partial \dot{n}_{o,v}}{\partial n_{o,g}}\right)_k\right] \tag{4.67}$$

The partial derivatives of the nitrous oxide gas moles are:

$$\left(\frac{\partial n_{o,g}}{\partial P_T}\right)_k = -dt\left[\zeta\left(\frac{\dot{n}_{o,f}}{\partial P_T}\right)_k + \left(\frac{\dot{n}_{o,v}}{\partial P_T}\right)_k\right] \tag{4.68}$$

$$\left(\frac{\partial n_{o,g}}{\partial T_T}\right)_k = -dt\left[\zeta\left(\frac{\dot{n}_{o,f}}{\partial T_T}\right)_k + \left(\frac{\dot{n}_{o,v}}{\partial T_T}\right)_k\right] \tag{4.69}$$

$$\left(\frac{\partial n_{o,g}}{\partial \dot{T}_T}\right)_k = dt\left[\left(\frac{\dot{n}_{o,v}}{\partial \dot{T}_T}\right)_k\right] \tag{4.70}$$

$$\left(\frac{\partial n_{o,g}}{\partial n_{o,l}}\right)_k = dt\left[\left(\frac{\dot{n}_{o,v}}{\partial n_{o,l}}\right)_k\right] \tag{4.71}$$

$$\left(\frac{\partial n_{o,g}}{\partial n_{o,g}}\right)_k = dt\left[\left(\frac{\dot{n}_{o,v}}{\partial n_{o,g}}\right)_k\right] \tag{4.72}$$

4.3.3 Jacobian of the System Model

The format for the system model Jacobian is presented here. The equations behind each term are listed below:

- Row 1: Equations 4.56, 4.57, 4.58, 4.58
- Row 2: Equation 4.59
- Row 3: Equation 4.60

- Row 4: Equations 4.61, 4.61, 4.61, 4.62
- Row 5: Equations 4.64, 4.65, 4.66, 4.67, 4.67
- Row 6: Equations 4.69, 4.70, 4.71, 4.72, 4.72

$$F_k = \begin{bmatrix} 0 & \left(\frac{\partial m_o}{\partial P_T}\right)_k & \left(\frac{\partial m_o}{\partial T_T}\right)_k & 0 & M_o & M_o \\ 0 & 0 & 0 & 0 & 0 & \left(\frac{\partial P_T}{\partial n_{o,g}}\right)_k \\ 0 & 0 & 0 & dt & 0 & 0 \\ 0 & \left(\frac{\partial \dot{T}_T}{\partial P_T}\right)_k & \left(\frac{\partial \dot{T}_T}{\partial T_T}\right)_k & 0 & \left(\frac{\partial \dot{T}_T}{\partial n_{o,l}}\right)_k & \left(\frac{\partial \dot{T}_T}{\partial n_{o,g}}\right)_k \\ 0 & \left(\frac{\partial n_{o,l}}{\partial P_T}\right)_k & \left(\frac{\partial n_{o,l}}{\partial T_T}\right)_k & \left(\frac{\partial n_{o,l}}{\partial \dot{T}_T}\right)_k & \left(\frac{\partial n_{o,l}}{\partial n_{o,l}}\right)_k & \left(\frac{\partial n_{o,l}}{\partial n_{o,g}}\right)_k \\ 0 & \left(\frac{\partial n_{o,g}}{\partial P_T}\right)_k & \left(\frac{\partial n_{o,g}}{\partial T_T}\right)_k & \left(\frac{\partial n_{o,g}}{\partial \dot{T}_T}\right)_k & \left(\frac{\partial n_{o,g}}{\partial n_{o,l}}\right)_k & \left(\frac{\partial n_{o,g}}{\partial n_{o,g}}\right)_k \end{bmatrix} \tag{4.73}$$

where F_k is the system model Jacobian Matrix at a discrete time step.

4.4 Extended Kalman Filter Structure

The implementation of the Extended Kalman Filter follows a standard structure and is shown below. At each time step, the system states, represented as $\hat{x}_{k|k-1}$, are estimated:

$$\hat{x}_{k|k-1} = f(\hat{x}_{k-1|k-1}, y_k, u_k) \tag{4.74}$$

Next, the approximation of estimate covariance, $P_{k|k-1}$, is predicted based on the prior time step's estimate covariance and the process noise, Q_k, of the current time step:

$$P_{k|k-1} = F_k P_{k-1|k-1} F_k' + Q_k \tag{4.75}$$

Now the filter performs an update based on the best estimates of the state and the current measurements. A measurement residual, $\tilde{y}_k$ is calculated:

$$\tilde{y}_k = y_k - H_k \hat{x}_{k|k-1} \tag{4.76}$$

where H_k is the measurement Jacobian Matrix.

Now an innovation covariance, S_k is determined:

$$S_k = H_k P_{k|k-1} H_k' + R_k \tag{4.77}$$

where R_k represents Gaussian measurement noise at a discrete time step.

The Gaussian measurement noise of the pressure sensor is determined by establishing a moving average value of the pressure data, and taking the standard deviation of the difference between the measured value and the moving average value. Using this method, the Gaussian noise value applied is 0.013. The Kalman gain, K_k, is determined:

$$K_k = P_{k|k-1} H_k' S_k^{-1} \tag{4.78}$$

The best estimate of the system states, $\hat{x}_{k|k}$, are now determined:

$$\hat{x}_{k|k} = \hat{x}_{k|k-1} + K_k \tilde{y}_k \tag{4.79}$$

The best covariance estimate, $P_{k|k}$, is also updated:

$$P_{k|k} = I - K_k H_k \tag{4.80}$$

This algorithm is used to provide both a state estimate and a covariance estimate from a state evolution model and a measurement.

4.5 Identifying Uncertainty for State and Measurement Updates

The primary task in tuning the Extended Kalman Filter is the proper selection of values for the process covariance matrix Q_k. In this particular implementation, the values of this matrix do not change over time. The matrix is composed of zeros with real, positive values on the primary diagonal. A Design of Experiment approach is used to determine the impact of each of these values. The diagonal is initially set to ones such that the matrix Q is an identity matrix. High and low values for each states process noise are established by multiplying and dividing each value on the diagonal by 10. This effectively increases or decreases the process noise for each state by an order of magnitude. It is determined that only the modeled process noise for the system pressure has an impact on the performance of the Extended Kalman Filter. This follows as no measurements for the other states are

considered in the Extended Kalman Filter. The performance of the Extended Kalman Filter is determined by the Mean Square Error between the estimated and measured mass of nitrous oxide.

For Case 2 data, changing the pressure process noise value from 1 to 10 increases the performance of mass history estimation by 3.48%. Further changing the pressure process noise from 10 to 100 increases the performance by 0.35%.

For Case 3 data, changing the pressure process noise value from 1 to 10 increases the performance of mass history estimation by 0.98%.

These results indicate that increasing the modeled process noise of the system pressure increases the accuracy of estimated mass history. It is further indicated that increasing the order of magnitude of the modeled process covariance beyond 10 has an increase in accuracy of less than 1%. Therefore, the recommended process covariance matrix is shown in 4.81.

$$Q = \begin{bmatrix} 1 & 0 & 0 & 0 & 0 & 0 \\ 0 & 10 & 0 & 0 & 0 & 0 \\ 0 & 0 & 1 & 0 & 0 & 0 \\ 0 & 0 & 0 & 1 & 0 & 0 \\ 0 & 0 & 0 & 0 & 1 & 0 \\ 0 & 0 & 0 & 0 & 0 & 1 \end{bmatrix} \tag{4.81}$$

4.6 Results of the Extended Kalman Filter

The results of the Extended Kalman Filter derived and tuned in this work are shown in the following figures. The Extended Kalman Filter can predict the remaining mass of nitrous oxide in the oxidizer tank to a reasonable level of accuracy. This is demonstrated by the close agreement in the measured and predicted values for oxidizer mass in figures 4.1 and 4.2.

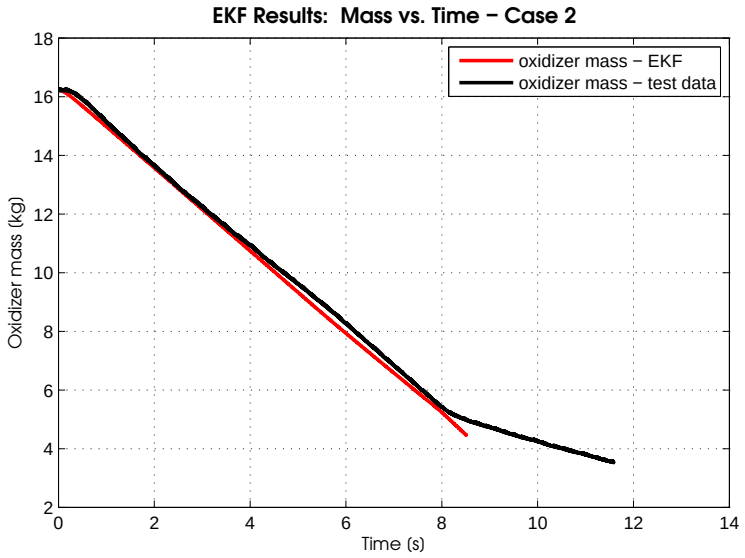

Figure 4.1: Oxidizer mass - Case 2: comparison of Extended Kalman Filter (EKF) and testing results

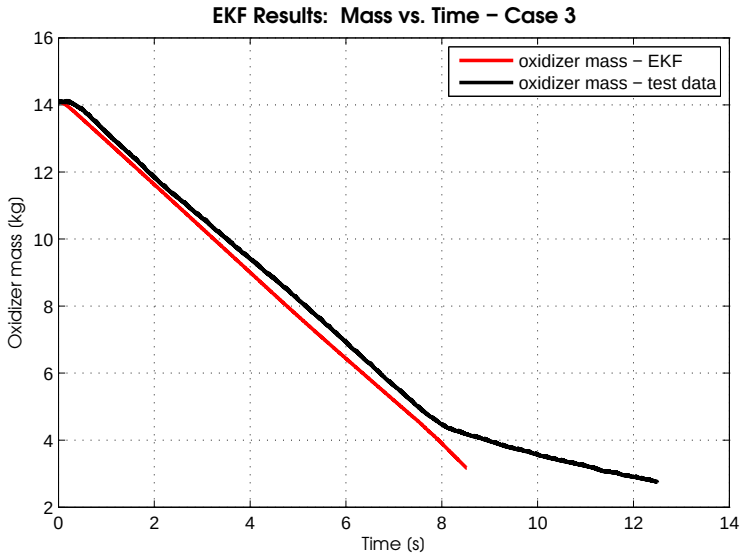

Figure 4.2: Oxidizer mass - Case 3: comparison of Extended Kalman Filter (EKF) and testing results

The Extended Kalman Filter returns almost exactly the measured pressure of the system. This is demonstrated in figures 4.3 and 4.4.

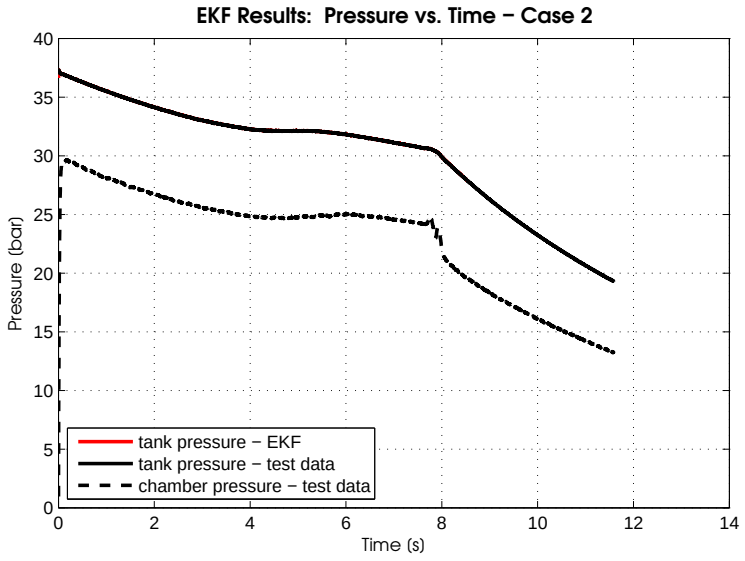

Figure 4.3: Pressure in oxidizer tank - Case 2: comparison of Extended Kalman Filter (EKF) and testing results

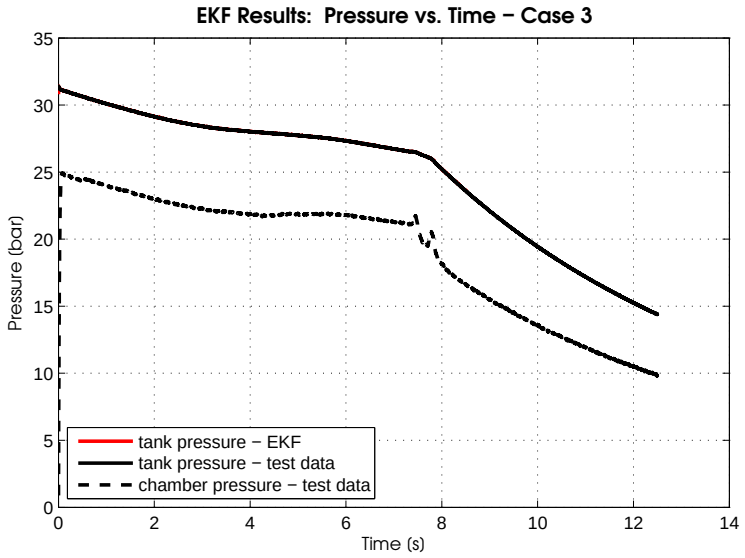

Figure 4.4: Pressure in oxidizer tank - Case 3: comparison of Extended Kalman Filter (EKF) and testing results

The temperature estimated by the Extended Kalman Filter is shown in figures 4.5 and 4.6.

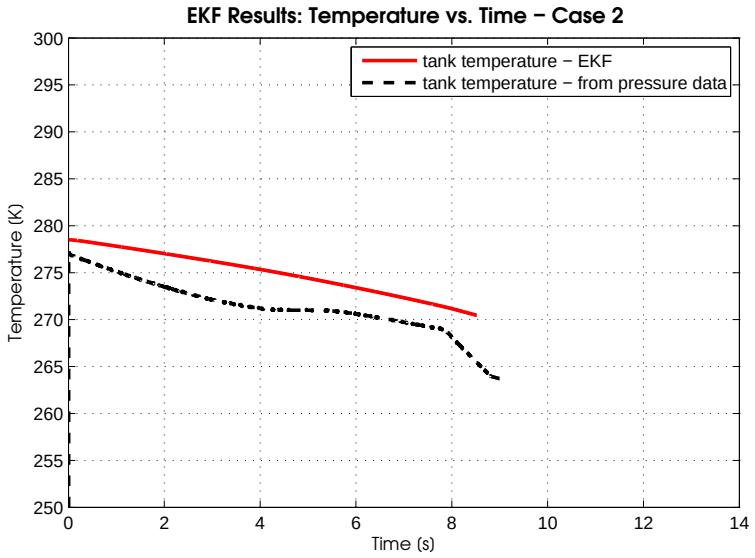

Figure 4.5: Oxidizer temperature - Case 2: comparison of Extended Kalman Filter (EKF) and estimations of temperature assuming saturation pressure

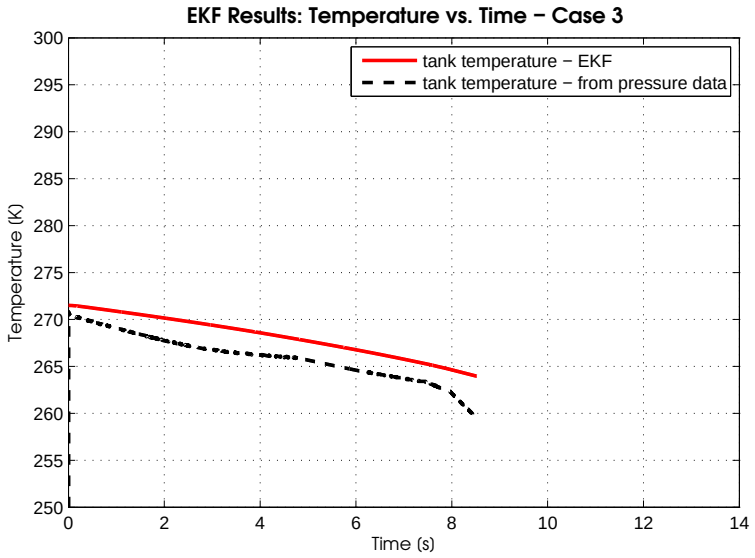

Figure 4.6: Oxidizer temperature - Case 3: comparison of Extended Kalman Filter (EKF) and estimations of temperature assuming saturation pressure

The liquid and gas moles of nitrous oxide are shown in figures 4.7 and 4.8. These are shown for completeness as the moles in the liquid and gas phases are states of EKF.

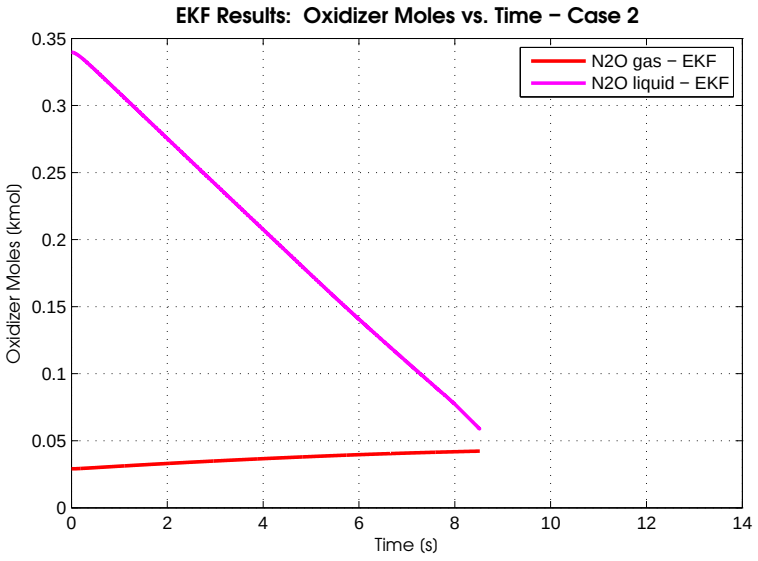

Figure 4.7: Moles of oxidizer phases - Case 2: Extended Kalman Filter (EKF) estimations

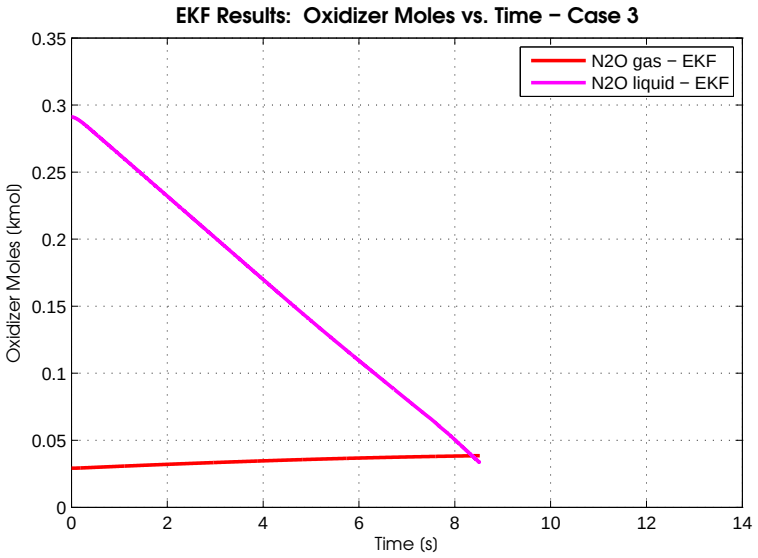

Figure 4.8: Moles of oxidizer phases - Case 3: Extended Kalman Filter (EKF) estimations

Chapter 5

Conclusions and Recommendations

In this work a modified model of nitrous oxide exiting an oxidizer tank is proposed. The modifications stem from the observation of an initial delay in the outflow, and from the assumption that the outflow is composed of a liquid and gas mixture. The modified model is implemented in an Extended Kalman Filter (EKF) that is capable of estimating the states and remaining mass of nitrous oxide in a tank. The contributions made to modeling an oxidizer tank are mentioned, followed by the use of an EKF for estimating the remaining nitrous oxide mass, and finally areas of potential refinement are discussed.

5.1 Model Modifications

The variable τ is introduced as a time constant in a first order delay. This delay models a gradual opening of the injector instead of an instantaneous opening. This assumption allows the model to be more accurate in predicting the mass history of the model. It is also possible that this value is specific to this particular hybrid engine and oxidizer tank. The variable ζ is used to model the gas to total outflow ratio as a fixed ratio. After optimization, this modification leads to a more accurate average estimation of the oxidizer outflow density; however, it is also obvious that the outflow density varies significantly during the draining of the oxidizer tank. After implementing the τ and ζ modifications in a model, the accuracy in modeling the mass history is significantly increased.

5.2 Extended Kalman Filter

An Extended Kalman Filter is proposed that estimates the total mass of nitrous oxide remaining in the oxidizer tank. The filter allows the remaining oxidizer mass to be estimated in the absence of direct measurement. The control inputs are the pressure in the combustion chamber and the product of the flow coefficient and cross-sectional area of the injector. The initial inputs are the total initial mass of oxidizer in the oxidizer tank and the initial temperature of the system, both are assumed to be measurable only on the launch-pad. The only updated measurement input in flight is the pressure in the oxidizer tank. It is arguable that the combustion chamber pressure should be considered a measurement rather than a control variable. In this embodiment of the EKF, it is convenient to consider the combustion chamber pressure to be a control variable and there is minimal cost to the performance and accuracy of the estimate. The oxidizer pressure is measured in the actual system; therefore, only the process noise of the modeled system pressure impacts the results of the EKF. In the covariance matrix, the EKF's reliance on the modeled pressure is reduced and the pressure state closely follows the measured pressure. The remaining oxidizer mass estimated by the EKF provides a much better estimation of mass in the oxidizer tank than a model alone. Increasing the accuracy of the EKF requires greater accuracy in the modeling of the system.

5.3 Future Potential Refinements

In the development of the model modifications and the EKF, several assumptions have been made. If the work of this thesis is applied to another hybrid rocket design, these assumptions should be reviewed. The flow through the injector should be reviewed for an outflow speed that nears or exceeds the speed of sound in oxidizer. If so, the equations governing the outflow should be modified appropriately, including an initial opening delay. Models of nitrous oxide properties are still being refined and developed. In the future, these models can be reviewed for accuracy and replacing assumptions with scientific understanding of the system. As an example, it is assumed that the nitrous oxide is in saturated equilibrium; however, this is not proven. The time required for the nitrous oxide to re-establish equilibrium may be long in comparison to the changes incurred by the dynamics of draining. More directly related to the work of this thesis, an understanding of the liquid and gas mixture in the injector is required to improve the understanding of the oxidizer tank dynamics. The two data sets show that the outflow density may fluctuate significantly over time; however, the current model does not simulate this dynamic behav-

ior. In the current work, it is assumed that the only updated observation comes from a sensor measuring the pressure in the oxidizer tank. In a future study, additional sensors could be added; the addition of temperature sensors in the oxidizer tank are an obvious example. The current EKF focuses only on the oxidizer tank. This approach could be further expanded to model the entire hybrid engine, including the combustion chamber and infrastructure between the tank and chamber. Other infrastructure would include an adjustable flow rate control mechanism, such as a valve. An EKF that extends the entire hybrid engine design could estimate the mass of not only the remaining oxidizer, but the remaining fuel as well. Further, it would be of use to the overall control of the rocket to estimate the moment of inertia of the hybrid engine and its center of mass. This approach could be further extended to the entire rocket where dynamic measurements of altitude, velocity, acceleration, and trajectory combined with a model of the entire rocket. This filter can be used to further correct the estimations of mass, center of mass, moments of inertia, drag and center of pressure. This information could be used in controlling the thrust and trajectory of the entire rocket. These refinements are left as future work.

5.4 Final Remarks

With this work, a relatively simple model of nitrous oxide draining from an oxidizer tank is now available. Further, this model is implemented in an Extended Kalman Filter that is now available for use. The sensors required are relatively standard, and are likely to be included in the engine design already. The filter can be implemented with an on-board computational device; no additional or elaborate systems are required. These hardware requirements should allow hybrid rocket engines to remain a controllable, low-cost, and safe launch system. This work will hopefully increase the accessibility of the upper atmosphere, low earth orbit, and space itself to lower budget programs. These programs may include research, weather prediction, satellites, and even manned missions.

References

[1] J. R. Wertz and W. J. Larson, Eds., *Space mission analysis and design*, 3rd ed. Torrance, CA: Microcosm, 1999.

[2] G. P. Sutton, *Rocket propulsion elements*, 7th ed. New York, NY: Wiley, 2001.

[3] A. Stamminger, J. Turner, M. Hrschgen, and W. Jung, "Sounding Rockets as a Real Flight Platform for Aerothermodynamic CFD Validation of Hypersonic Flight Experiments." Cologne, Germany: European Space Agency, Nov. 2005.

[4] G. N. Henry, W. J. Larson, and R. W. Humble, *Space Propulsion Analysis and Design*. New York, NY: McGraw-Hill, 1995.

[5] L. C. Saindon, "Development of Oxidizer Flow Control for use in Hybrid Rocket Motors of the Scientific Sounding Rocket Scale," Undergraduate, University of Maine, Orono, ME, 2012. [Online]. Available: http://digitalcommons.library.umaine.edu/honors/33

[6] Z. W. Peterson, "Closed-Loop Thrust and Pressure Profile Throttling of a Nitrous Oxide/Hydroxyl-Terminated Polybutadiene Hybrid Rocket Motor," M.S., Utah State University, Logan, UT, 2012. [Online]. Available: http://digitalcommons.usu.edu/etd/1400

[7] J. E. Zimmerman, B. S. Waxman, B. J. Cantwell, and G. G. Zilliac, "Review and Evaluation of Models for Self-Pressurizing Propellant Tank Dynamics," in *49th AIAA/ASME/SAE/ASEE*, vol. 2013-4045. San Jose, CA: American Institute of Aeronautics and Astronautics, Inc.,, 2013, p. 24.

[8] P.-J. Bristeau and N. Petit, "Trajectory estimation for a hybrid rocket." Chicgo, IL: American Institute of Aeronautics and Astronautics, Inc.,, Aug. 2009.

[9] K. I. Platt, "Design and Fabrication of a Full-Featured Labscale Hybrid Rocket Engine," M.S., University of Central Florida, Orlando, FL, 2006. [Online]. Available: http://etd.fcla.edu/CF/CFE0000972/Platt_Kyle_I_200605_MS.pdf

[10] M. J. Chiaverini and K. K. Kuo, Eds., *Fundamentals of hybrid rocket combustion and propulsion*, ser. Progress in astronautics and aeronautics. Reston, VA: American Institute of Aeronautics and Astronautics, 2007, vol. 218.

[11] M. A. Karabeyoglu, G. G. Zilliac, B. J. Cantwell, S. De Zilwa, and P. Castellucci, "Scale-Up Tests of High Regression Rate Liquefying Hybrid Rocket Fuels," in *41st Aerospace Sciences Meeting and Exhibit*. Reno, NV: American Institute of Aeronautics and Astronautics, Jan. 2003.

[12] B. S. Waxman, J. E. Zimmerman, B. J. Cantwell, and G. G. Zilliac, "Effects of Injector Design on Combustion Stability in Hybrid Rockets Using Self-Pressurizing Oxidizers," in *Propulsion and Energy Forum*, Cleveland, OH, Jul. 2014.

[13] T.-V. Chelaru and F. Mingireanu, "Hybrid Rocket Engine, theoretical model and experiment," *Acta Astronautica*, vol. 68, no. 11-12, pp. 1891–1902, 2011.

[14] M. M. Fernandez, "Propellant Tank Pressurization Modeling for a Hybrid Rocket," MS, Rochester Institute of Technology, Rochester, NY, 2009. [Online]. Available: http://scholarworks.rit.edu/cgi/viewcontent.cgi?article=8116&context=theses

[15] B. J. Solomon, "Engineering Model to Calculate Mass Flow Rate of a Two-Phase Saturated Fluid Through An Injector Orifice," M.S., Utah State University, Logan, UT, 2011. [Online]. Available: http://digitalcommons.usu.edu/gradreports/110

[16] J. E. Zimmerman, B. S. Waxman, B. J. Cantwell, and G. G. Zilliac, "Comparison of Nitrous Oxide and Carbon Dioxide with Applications to Self-Pressurizing Propellant Tank Expulsion Dynamics," 2013. [Online]. Available: http://spase.stanford.edu/Self-Pressurizing_Propellant_Dynamics_files/Zimmerman%20et%20

[17] J. E. Zimmerman, "Self-Pressurizing Propellant Tank Dynamics," Ph.D, Stanford University, Stanford, CA, Dec. 2015. [Online]. Available: file:///C:/Users/sjbor_000/Downloads/main_adob-augmented.pdf

[18] B. Genevive, M. J. Brooks, J.-F. P. Pitot de la Beaujardiere, and L. W. Roberts, "Performance Modeling of a Paraffin Wax / Nitrous Oxide Hybrid Rocket Motor," in *Aerospace Sciences Meetings*, Orlando, FL, Jan. 2011. [Online]. Available: http://enu.kz/repository/2011/AIAA-2011-420.pdf

[19] R. H. Perry, D. W. Green, and J. O. Maloney, *Perry's Chemical Engineers' Handbook*, 7th ed. New York, NY: McGraw-Hill, 1997.

[20] F. M. White, *Fluid Mechanics*, 6th ed. New York, NY: McGraw Hill, 2008.

[21] G. G. Zilliac and J. E. Zimmerman, "Personal Correspondence," Nov. 2014.

[22] ——, "Personal Correspondence," Jun. 2015.

[23] J. E. Zimmerman, B. J. Cantwell, and G. G. Zilliac, "Initial Experimental Investigations of Self-Pressurizing Propellant Dynamics," in *48th AIAA/ASME/SAE/ASEE Joint Propulsion Conference & Exhibit*. Atlanta, GA: American Institute of Aeronautics and Astronautics, Inc.,, 2012.

[24] M. J. Anderson and P. J. Whitcomb, *DOE Simplified: Practical Tools for Effective Experimentation*. Portland, OR: Productivity Press, 2000.